Assessing two methods to define rainfall intensity and duration thresholds for shallow landslides in data-scarce catchments of the Colombian Andean Mountains

Roberto J. Marin [a,b], María Fernanda Velásquez [a,b], Edwin F. García [b], Massimiliano Alvioli [c], Edier Aristizábal [d].
Corresponding author: Roberto J. Marin. E-mail: rjose.marin@udea.edu.co. Phone: +57 3015299839.
[a] Landslide Scientific Assessment (LandScient), Medellín, Colombia.
[b] Universidad de Antioquia-UdeA, Escuela Ambiental, Facultad de Ingeniería, Grupo de Investigación en Infraestructura (GII), Calle 70 No. 52-21, Medellín, Colombia.
[c] Consiglio Nazionale delle Ricerche, Istituto di Ricerca per la Protezione Idrogeologica, via Madonna Alta 126, I-06128, Perugia, Italy.
[d] Universidad Nacional de Colombia, Sede Medellín, Departamento de Geociencias y Medio Ambiente, Carrera 80 No 65-223, Medellín - Colombia.

Abstract

Rainfall thresholds are intensity-duration relations supposedly able to distinguish precipitation events that may or may not trigger landslides. The most common method for defining rainfall thresholds relies on observed landslides and the corresponding values of rainfall intensity and duration that caused each failure. Alternative methods to define rainfall thresholds, using physically-based models, recently gained importance, as they may provide complementary information to other methods. Still, their applicability in most of the world's regions, including the Colombian Andes' mountainous basins, has not been demonstrated or validated. In this study, we evaluated the applicability of the physically-based model TRIGRS to define rainfall intensity and duration thresholds in individual basins from the Colombian Andes. We obtained rainfall thresholds using two different methods and compared them with landslide-triggering rainfall events in two distinct basins, namely La Arenosa and La Liboriana. Furthermore, we used a (presumably incomplete) landslide database from Medellín to rebuild the rainfall events associated with individual landslides and compared them with the physically-based thresholds. The rainfall thresholds calculated in the three study areas and the applicability of the methods in data-scarce environments were assessed. Results showed that both methods for defining rainfall intensity and duration thresholds have merits and represent potential tools to improve or complement landslide early warning systems, especially in data-scarce regions.

Keywords: rainfall threshold, landslides, early warning system, data-scarce region, TRIGRS, numerical modeling

1. Introduction

Rainfall-induced landslides are very common in mountain terrains worldwide, causing numerous casualties and economic losses in many countries. Nevertheless, most affected territories lack a landslide early warning system (LEWS) to prevent or mitigate their disastrous consequences (Guzzetti et al., 2020). One reason for that could be the complexity involved in its development, including a solid organization and contribution from several specialists in diverse knowledge areas (Intrieri et al., 2013). Scientific, economic and technological advancement is still required to increase the reliability and efficacy of existent and future LEWSs.

Since rainfall is the most frequent triggering cause of landslide initiation (Chatra et al., 2019; Vessia et al., 2020; Zhao et al., 2020), rainfall thresholds are usually a key component in the mechanism of LEWSs. Thresholds represent rainfall conditions (*e.g.*, duration, intensity, cumulated or antecedent rainfall) that could trigger landslides when the threshold is reached or exceeded (Guzzetti et al., 2008). Thus, rainfall thresholds for landslides identify the "minimum" conditions associated with the occurrence of these instabilities. The goal of applying thresholds is forecasting landslide occurrence in a given terrain and for a given antecedent rainfall conditions. Most scientific literature studies are restricted to particular areas, though the scale of different studies may vary largely. Application at local scale (generally few km^2 up to some hundreds) represents 24.2% of existing studies, and 39.2% are defined at basin scale (hydrographic river of a basin) (Segoni et al., 2018). Most of the existing studies defined thresholds using probabilistic approaches (Brunetti et al., 2010; Melillo et al., 2020).

The preparation and validation of rainfall thresholds intended to forecast landslide initiation are severely limited when landslide inventories are incomplete and accurate rainfall triggering conditions at the location and time of occurrence lack. Physically-based models represent another possible approach besides the empirical-statistical methods (Papa et al., 2013; Alvioli et al., 2014; Salciarini and Tamagnini, 2015; Alvioli et al., 2018; Marin 2020; Marin and Velásquez, 2020; Bordoni et al., 2019; Zhao et al., 2019; 2020). They could be particularly useful where empirical-statistical methods cannot be used for the absence of suitable data, particularly in small areas (<1 km^2). Conversely, a difficulty for physically-based methods is the necessity of adequate geotechnical and hydraulic input parameters required in numerical modeling.

Examples of physically-based rainfall thresholds, including validation of the curves, exist in the literature. Zhao et al. (2019, 2020) applied physically-based and statistical-empirical methodologies for landslide occurrence in the Emilia-Romagna region (Italy). They compared them with landslide records simulating the moisture condition using the distributed hydrological model SHETRAN (Ewen et al., 2000). The two basins used in both research studies have relatively large areas (1,191 km^2 and 742 km^2).

Bordoni et al. (2019) compared statistical-empirical and physically-based thresholds obtained with TRIGRS with shallow landslide triggering duration and cumulated precipitations in a hilly area from Oltrepò Pavese (Italian Apennines). The physically-based thresholds were defined using a representative test-site (apparently an area <0.5 km^2, not stated in the paper) that they justified having the typical geological and geomorphological predisposition to landslide occurrence for the rest of the study area. Even though the whole area has various geological units with different mechanical and hydraulic properties, the different thresholds (according to certain initial water-pressures: -20 kPa, -10 kPa and 0 kPa) were validated using events from all the study area (265 km^2). It differs from considering that a specific study site's thresholds should not be extended to a different area (Marin et al., 2020). Still, great importance is regarded to define thresholds depending on the antecedent rainfall and soil moisture circumstances due to their high influence on the slope stability and the thresholds' characteristics (Marin and Velásquez, 2020).

Examples of landslide assessment studies in the mountainous regions of the Colombian Andes show both physically-based (Aristizábal et al., 2016; Marin and Mattos, 2020; Martínez-Carvajal et al., 2018; Vega and Hidalgo, 2016) or statistical (Grima et al., 2020; Ramos-Cañón et al., 2016) approaches. In the region, landslide data is not abundant, and further validation of physically-based methods to define rainfall intensity-duration thresholds for shallow landslides, as the recently proposed and implemented (Marin, 2020; Marin et al., 2020; Marín et al., 2019; Marin and Velásquez, 2020), is still required.

This research aims to compare two physically-based methodologies (one at basin scale and the other at grid cell scale) to define rainfall intensity-duration thresholds and evaluate their applicability in data-scarce environments from the Colombian Andes. To this end, we compared thresholds obtained using both methods with landslide-triggering rainfall events in two well-known case studies of groups of shallow landslides detonated by extreme rainfalls. The study areas and events are in the La Arenosa basin, San Carlos, September 21st, 1990, and the La Liboriana basin, Salgar, May 15th, 2015, both in Colombia. That represents a direct evaluation of the thresholds' performance (rainfall-induced shallow landslide predictive capacity). Moreover, we carried out an analysis of individual landslides in small watersheds in the Medellín area. We investigated the possibility of inferring rainfall-triggering conditions, using antecedent precipitation data starting from two days before the landslide report. Rainfall thresholds using both mentioned physically-based methods were defined and compared with the reconstructed triggering events.

2. Study areas

2.1 San Carlos

The La Arenosa basin (San Carlos, Antioquia) is situated in the Cordillera Central (Colombian Andean Mountains). The location of the basin is presented in Fig. 1. It has an average annual precipitation of 4,300 mm, distinctive of a humid tropical climate. The rainfall pattern can be considered bimodal, with the first rainy season in March, April and May and then in September, October and November. The average annual temperature is 23 °C. Its surface area is approximately 9.91 km^2, where elevations vary from approximately 1,000 to 1,900 m.a.s.1. The predominant slopes of the terrain range between 20° and 40°.

There are three geomorphological units in the basin. The steep slopes, which constitute the upper zone of the basin (slopes greater than 26.6°); slopes on saprolite, corresponding to moderately steep slopes (slopes less than 19.3°) and the colluvial-alluvial plain, topographically corrugated and not very steep (slopes around 5.7°) (ISA et al., 1991). The geology comprises residual soils of the Antioquian Batolito's granodioritic rocks covering areas of gentle slopes with fluvial-torrential deposits (Mejía and Velásquez, 1991).

The rainfall event that caused the La Arenosa basin's failures corresponds to the short duration and high-intensity event on September 21st, 1990, when the total rainfall of 208 mm in less than 3 h occurred. It triggered many shallow landslides. Mejía and Velásquez (1991) reported more than 800 soil slips from which almost 700 caused debris flows, impacting families and infrastructures (houses, roads, bridges and the Calderas Hydroelectric Power Plant (Aristizábal et al., 2015, 2016). Soil thicknesses ranged from 1 m to 2.7 m, in which thin soil was found on narrow ridges, and thick soils and colluviums accumulated at the bottom of the valleys (Aristizábal, 2013). Fig. 2 presents the geological units in the study area and a partial landslide inventory (scarps) of the September 21st, 1990 event, which was mapped using visual image interpretation of aerial photographs taken after the event.

2.2 Salgar

The La Liboriana basin (southwestern Antioquia, Colombia) is in the Cordillera Occidental (Colombian Andean Mountains), at the base of Cerro Plateado. Fig. 3 shows the location of the basin. The region has a humid tropical climate and an average annual rainfall of 2,000 mm. The area's precipitation regime is considered bimodal (same as San Carlos), with higher precipitations in May and October. It has a mean temperature of 23 °C (approximately). The basin's surface extension is approximately 59 km^2, but the upper part of the basin where we applied the methods to define thresholds has and area of 5.2 km^2. Elevations vary from 1,236 to 3,722 m.a.s.l. with slope gradients mainly ranging from 20° to 40°, and few steeper slopes exceeding 70°, located mostly in the upper (north-western) part of the basin.

The geomorphology in the basin is characterized by a rugged mountainous area in the upper part, narrow valleys and steep forested slopes (Ruiz Vásquez, 2017). Geologically, much of the area contains sedimentary rocks from the Upper Cretaceous (Kaa). Specifically, the Urrao member of the Penderisco Formation, made up of chert strata (SGC, 2014a; SGC, 2014b), and intrusive igneous rocks from the Miocene (Tdt) and Quaternary deposits (Qar).

The heavy rainfall event that caused the landslide cluster in the north-western portion of the study site corresponds to the rainfall event in May 17-18th, 2015. Shallow landslides (soil slips) and debris flows movilized different sediments (mud, plants and stones) with great velocity (advancing with increasing power) and affecting part of Salgar. The total rainfall was 160 mm in less than 20 h, causing casualties and infrastructure damage. Fig. 4 shows the geological units in the study area and the landslide inventory (scarps of the soil slips identified using satellite images) of the May 18th, 2015 event.

2.3 Medellín

Medellín is situated in the Valle de Aburrá, in the Central Cordillera of the Colombian Andean (Fig. 5). The Valle de Aburrá is a deep valley in complex and tropical terrains. The central and lower section of the valley is characterized by alluvial plains, constrained by moderate step-like slopes and strongly dissected local tributary valleys (Aristizábal et al., 2005). The geomorphology of the valley changes marginally from south to north. The southern part of the valley is asymmetrical and narrow with steep slope gradients. On the other hand, the northern part of the valley is symmetrical and narrow, also with steep slope gradients. Rainfall has a bimodal pattern in annual time scale and varies from 1,000 mm to 3,000 mm, with peaks of precipitation in April-May and October-November.

Geologically, the valley is composed of a metamorphic belt composed of gneisses, schists, and amphibolites, thrust by ultrabasic rocks such as dunites and gabbros (Toussaint and Restrepo, 1994). The metamorphic rocks are intruded by plutonic bodies of acid to intermediate composition (Restrepo and Toussaint, 1984). In the lower/middle hillslopes, those rocks are covered by unconsolidated sediments, forming a complex of ancient debris flow and fluvial deposits.

Fig 5 shows the location of 6 watersheds (W1-W6) from Medellín studied in this research work, which have different geological setting. Fig. 6 shows the geology of those small watersheds. Watershed 1 (W1) and watershed 2 (W2) share some geological units, among them the Medellín Dunites (JKuM), which are part of the Aburrá Ophiolithic complex, with a low thickness weathering profile. There are also some anthropogenic fills (QII), which are fill materials or debris due to the high urban and construction growth. In addition, there are some debris and/or mudflow deposits (NQFII, QFIV and NFI). The QFIV (corresponds to the most recent deposit) and the NFI is only found in W2. Additionally, W1 has a geological unit called Stock de Las Estancias (KcdE), corresponding to minor granitoid bodies of the Antioquian Batolite (intrusive massive body) of predominantly sandy silt granulometry. Finally, in W2 there is an alluvial-torrential deposit (Qat), deposits resulting from torrential floods, where materials of varied granulometry (from blocks to clays) are mixed with a landslide deposit (Qd), they are small landslides and most of them present rock fragments of the size of gravel and blocks embedded in a fine-grained matrix.

W3 and W4 share most of the geological units. Both are formed by the San Diego Stock (KgSD), basic plutonic igneous rocks, which exhibit an advanced weathering process with predominantly silt-clay soils. The Medellín Amphibolites (TRaM) are also found, which exhibit a granulometry ranging from silt, clayey silt to clay in the most surficial layer (VI). Debris flow and/or mudflows deposits are also present, specifically recent deposits called QFIV (W3) and QFIII. Those watersheds have small portions of anthropogenic fills (QII). The geological units of W5 and W6 are the Volcanosedimentary Member (KvsQG) (Quebradagrande Complex), which are black siliceous shales in a siliceous clayey mass with a large amount of organic material. There are also two debris and/or mudflow deposits, the NQFII and NFpreI (older deposit). A small alluvial-torrential deposit (Qat) is also found in W5.

3. Available data

3.1 Topographic data

Digital elevation models (DEM) for the La Arenosa basin and Medellín watersheds were obtained from the Instituto Geografico Agustin Codazzi (IGAC). Both DEMs have a grid cell size of 10 m, consistent with the spatial resolution of the geological unit maps available for both territories. The DEM for the La Liboriana basin (Salgar) was downloaded from ALOS-PALSAR (ASF, 2015), with a grid cell size of 12.5 m.

3.2 Parameterization of geotechnical and hydraulic parameters

Table 1 lists the geotechnical and hydraulic soil parameters of the La Arenosa basin (Marin et al., 2021a) used in this work. The mechanical parameters were obtained from soil descriptions and analyses carried out by INTEGRAL (1990) and Mejía & Velásquez (1991) from laboratory tests and field data at the study site after the landslide events on September 21st, 1990. Aristizábal et al. (2015, 2016) defined the soil's hydraulic and geotechnical properties in the study area. According to their soil types, additional parameters such as the saturated hydraulic conductivity (required by the physically-based modeling) were defined based on typical scientific literature values (Chowdhury, 2010; Huang, 2012; Das, 2013; Budhu, 2015; Ghanbarian and Hunt, 2017), correlations (e.g. hydraulic diffusivity) and/or pedotransfer functions (PTFs, for the soil water retention curve, explained in the Section 4.3).

Table 2 lists the geotechnical and hydraulic soil parameters for the La Liboriana basin (Marin et al., 2021b) used in this work. Values in Table 2 were obtained through a back-analysis of the May 18th, 2015, shallow landslide events. This study site's input data was very scarce; initial values of the parameters before back analysis were selected considering typical ranges from the literature for the soil types, as in Marin et al. (2021b). Geological descriptions of the predominant soils (clay loam and sandy soil) of the study site were used to define initial values of the hydraulic and mechanical parameters for the back analysis. Back analysis consists in calibration/modification of the input values through repeated simulations using TRIGRS, until the results for F_S and the observed landslides match as closely as possible. The landslide scarp inventory, the rainfall event data and the factor of safety (F_S) results calculated with TRIGRS were used to perform ROC analyses as a function of the input parameters, maximizing agreement between results of simulations and observations. More details about the back analysis and how this scarce of data are evidently a drawback to obtain accurate results in the slope stability assessment were described by Marin et al. (2021b). It also affects the accuracy of the rainfall thresholds defined in this research paper.

Table 3 lists the geotechnical and hydraulic input parameters used for the landslide modeling for each geological unit of the watersheds from Medellín. Values in Table 3 were defined based on previous landslide susceptibility and hazard assessments in the Valle the Aburrá (AMVA, 2016; AMVA and UNAL, 2018), comparing the characterizations of the geological units in the watersheds from Medellín with representative values found in the literature. The number of landslides (and scarps) per unit area of each geological unit from a regional landslide inventory (SIMMA, 2021) was calculated to evaluate the historical likelihood of landslide occurrence. Each geological unit's landslide likelihood was used to adjust the mechanical parameters (c', φ', γ_s) compared with each geological unit's instabilities, performing F_S calculations assuming different pressure head values. The F_S results were compared with the total number of landslide scarps per unit area of the geological units, verifying that the geological units with more landslides per unit area (considered more prone to landslide occurrence) had lower F_S values than the geological units with less landslides per unit area. This process was executed repeatedly, and the best match between the landslide inventory and the F_S results was selected. To verify that the combination of values associated with the geotechnical parameters is as representative as possible with the expected soil response, a ROC analysis was performed after simulations with TRIGRS.

It was also verified that the input parameters used in the model represent soils with factors of safety greater than or equal to unity ($F_S \geq 1$) in most of the terrain before the simulated rainfall event, ensuring that the areas considered unstable ($F_S < 1$) are actually due to rainfall, and are not unconditionally unstable within the TRIGRS model.

For all the study sites in this research study (catchments in Salgar, San Carlos and Medellín), the saturated hydraulic diffusivity (D_0) was calculated as 100 K_s, as applied in other research studies with TRIGRS (Marin et al., 2020a; Tran et al., 2017).

4. Methods

4.1 The TRIGRS slope stability model

TRIGRS (Transient Rainfall Infiltration and Grid-Based Regional Slope-Stability) is a physically-based model that has been used worldwide in the scientific literature (Alvioli et al., 2018; Ciurleo et al., 2019; He et al., 2021; Weidner et al., 2018). The program is freely available, and it was originally developed at the United States Geological Survey, USGS (Baum et al., 2002). It was upgraded by Baum et al. (2008) and then by Alvioli and Baum (2016). TRIGRS is a time-dependent, distributed model based on the infinite slope approximation. In this research work, we used the finite depth model in unsaturated soil conditions.

TRIGRS calculates both the transient changes in pore water pressure and the factor of safety as a result of rainfall infiltration, generating the temporal and spatial distribution of shallow landslides. TRIGRS simulates transient water infiltration in unsaturated soils using the Richards equation's analytical solution (1931). Excess water produced in the infiltration process is diverted to adjacent areas of lower slopes that are more permeable, employing an optional surface runoff routing algorithm (Baum et al., 2008).

The SWRC is simulated by Gardner's exponential model (1958). An approximation of the effective stress is obtained as proposed by Vanapalli and Fredlund (2000) to define, in a simplified way, the effect of suction in the unsaturated zone. The model has a high dependence on the hydraulic conductivity and the water content, which is shown in the Richards equation, as follows:

$$\frac{\partial \theta}{\partial t} = \frac{\partial}{\partial Z}\left[K(\psi)\left(\frac{1}{\cos^2\delta}\frac{\partial \psi}{\partial Z} - 1\right)\right], \tag{1}$$

where ψ is the pressure head, Z the soil depth, θ the volumetric water content, t the time, δ the slope angle, and $K(\psi)$ is a function of the unsaturated hydraulic conductivity of the soil, defined as:

$$K(\psi) = K_s\, exp(\alpha_G\, \psi^*), \tag{2}$$

$$\theta = \theta_{res} + (\theta_{sat} - \theta_{res})exp(\alpha_G\, \psi^*), \tag{3}$$

where K_s is the saturated hydraulic conductivity, θ_{sat} the saturated volumetric water content, θ_{res} the residual volumetric water content, and α_G a parameter (inverse of the vertical height of the capillary fringe above the groundwater level), and $\psi* = \psi - \psi_0$; with ψ_0 as a constant ($\psi_0 = -1/\alpha$ or $\psi_0 = 0$).

Besides, TRIGRS assumes a homogeneous material for both unsaturated and saturated conditions, which allows the use of a simple infinite slope model to calculate the factor of safety (Taylor 1948). Thus, the factor of safety is calculated in the model as follows:

$$F_S(Z,t) = \frac{\tan\phi'}{tan\delta} + \frac{c' - \psi(Z,t)\gamma_W tan\phi'}{\gamma_S Z sen\delta cos\delta}, \tag{4}$$

where c' is the effective soil cohesion, ϕ' the effective friction angle, γ_w the unit weight of water, γ_s the unit weight of soil. A complete explanation of TRIGRS can be found in the software manual (Baum et al. 2008) and the latest version (v2.1) of the model (Alvioli and Baum, 2016).

4.2 Rainfall thresholds

Several authors (Alvioli et al., 2014; Salciarini and Tamagnini, 2015; Alvioli et al., 2018; Bordoni et al., 2019; Fusco et al., 2019) applied TRIGRS to determine the critical rainfall conditions (intensity-duration, *I-D*) that trigger potential shallow landslides. The two methodologies implemented in this study to define rainfall thresholds associated with shallow landslides in various mountainous basins of the Colombian Andean Mountains, using TRIGRS, are described below. The main difference between the two methods is how thresholds are defined: we defined them at the basin scale in the first method and at the grid cell scale in the second method.

The first method (in the following, M1) was originally proposed by Marin and Velásquez (2020), and it is based on the value of a critical area, a_c, for each basin. A basin is considered unstable if, after applying TRIGRS using a given rainfall series (*i.e.*, a rainfall event), the total area of grid cells with FS < 1, Δa_f, is larger than a_c. The critical failure area does not consider unconditionally unstable grid cells, *i.e.*, cells with $F_S < 1.0$ even without rainfall. We defined rainfall thresholds using different values of a_c: 0.1%, 0.15%, 0.2%, 0.3%, 0.5%, 0.7%, 0.9%, 1%, 1.5%, 3%, 5%, 7%, 9%, 10%, and 20% of the total area of the basin.

To obtain the rainfall thresholds, TRIGRS was run for a rainfall duration value, and the intensity (*I*) was increased (1 mm/h, from 0 to 200 mm/h) until the critical failure condition was reached (intensity-duration values that led to overall basin instability, $\Delta a_f \geq a_c$). The duration (*D*) was then increased, repeating the procedure to find the duration-intensity combinations that led to the condition $\Delta a_f \geq a_c$. The critical intensity is calculated interpolating (linearly) the intensity that relates the a_c value from the intensities that caused lower and higher Δa_f values (concerning a_c). We found that critical intensity changes over long periods and changes are not significant (the critical intensity becomes almost constant). Therefore, rainfall duration values above 10 h were not considered, limiting the range of duration of the threshold to this final duration (D_f).

We fitted the combinations of critical *I-D* values with a power-law:

$$I = \alpha D^{\beta}, \tag{5}$$

which we linearized as follows:

$$log\, I = \beta log\, D + log\, \alpha, \tag{6}$$

where D is the rainfall duration, I the average rainfall intensity, α, β the intercept and shape parameters of the power-law threshold curve, Eq. (5).

For the practical application of method M1, we resorted to a Python program developed by Marin and Velásquez (2020). The program runs TRIGRS for different combinations of input conditions. The program calculates the failing area from the output Fs map obtained after the simulations, storing the critical *I-D* conditions that produced $\Delta a_f \geq a_c$. Then, the program calculates the power-law equation using the ensemble of critical *I-D* values and plots the *I-D* thresholds.

In the second method (in the following, M2), the thresholds (*I-D*) are calculated for each grid cell of the study site (distributed thresholds), at variance with method M1, which define a threshold for the entire study area (basin thresholds).

For a given duration, TRIGRS was run by increasing the intensity from 0 mm/h to 200 mm/h. The critical *I-D* values that caused the failure ($F_S < 1.0$) to a grid cell were stored for each basin's specific cell. The critical intensity corresponds to the I value for which $F_S = 1.0$, obtained using a linear interpolation including the preceding I value (to the intensity that caused instability) and their corresponding F_S. The result is a critical intensity and duration data sets for each cell. The critical *I-D* data sets (for each grid cell) were fitted to the power-law Eq. (5), and the same linear transformation as method M1, Eq. (6), to represent the data in linear regression form, was performed, using least-squares linear regression to convert back to the power-law Eq. (5).

A Python program developed by Marin (2020) was used to implement M2, outlined above. The program calculates the critical rainfall conditions that trigger failures in each grid cell at the study site. It also generates maps of initial duration, D_i, and final duration, D_f, representing the anchor values to define each grid cell's threshold. The initial duration is the lowest value of D for which $F_S < 1.0$ in the given cell, and the final duration was set to 60 h. The rainfall threshold is applicable only in the duration range singled out by the values of α and β. By construction, within method M2, not all grid cells in a study area can be associated with a threshold.

In both methods, M1 and M2, we selected values of duration 1 h < D < 60 h (*cfr*. Table 4), and intensity values 1 mm/h < I < 200 mm/h.

4.3 Soil depth, initial groundwater level, soil-water retention curve

The model TRIGRS, used throughout this work, requires, among other inputs, a map of soil depth if the finite depth model is selected (as in this research study). Soil depth is defined as the boundary of the surficial layer with an assumed impermeable layer. The model also requires an initial depth for the groundwater level, which was set at the same soil depth boundary.

For the La Arenosa basin, we used an existing definition of the soil depth map, which was estimated as a function of the slope angle (δ) (Aristizábal, 2013). The map was obtained interpolating soil depth data at different points located in the basin, and the interpolating equation reads as follows:

$$d_{lz} = -0.026\ x\ \delta\ +\ 2.83, \tag{7}$$

which provided valued of depth 2.0 m < d_{lz} < 2.8 m, for alluvial soil, and 1.2 m < d_{lz} < 2.8 m, for residual soil. For the study sites in Salgar and Medellín, the soil depth maps were calculated as a function of the slope gradient and maximum/minimum soil thicknesses, as presented by Saulnier et al. (1997) as follows:

$$d_{\mathrm{lz}} = \mathrm{z}_{\max}\left[1 - \frac{\tan\delta - \tan\delta_{\min}}{\tan\delta_{\max} - \tan\delta_{\min}}\left(1 - \frac{\mathrm{z}_{\min}}{\mathrm{z}_{\max}}\right)\right], \tag{8}$$

where z_{max} and z_{min} are the maximum and minimum values of the surface soil thickness, δ_{min} and δ_{max} are the minimum and maximum slope angle values. The dependence of depth from the slope angle In Eq. (8) was also used by Tran et al. (2018).

For the La Liboriana basin, z_{max} = 2.2 m and z_{min} = 0.6 m were used for Tdt, and for Kaa values of z_{max} = 1.2 m and z_{min} = 0.8 m. These values resulted from the back-analysis carried out by Marin et al. (2021b) and the soil thickness descriptions in this study site, carried out by Osorio (2008).

For Medellín, the z_{max} values were obtained from the descriptions of soil horizons of the geological units in the studies by AMVA and UNAL (2018) in the municipalities of Valle de Aburrá (1.0 m < z_{max} < 4.0 m). The values correspond to the thickness of the soil's shallowest horizon presented in Dearman's (1991) weathering profile for each geological unit. For all geological units, it was set a z_{min} value of 0.2 m.

For all the study sites, the initial groundwater table was assumed at the same lower impermeable basal limit (soil depth, d_{lz}), following many studies with TRIGRS in the literature (Montrasio et al., 2011; Park et al., 2013; Tran et al., 2018; Baumann et al., 2018; Marín et al., 2019).

For the soil water retention curve (SWRC) parameters (θ_s, θ_r, α_G), we followed the model of Gardner (1958). The parameters were adjusted to the SWRC parameters of van Genuchten's (1980) model for tropical soils provided by Hodnett and Tomasella (2002) in all of the study sites (Medellín, La Liboriana and La Arenosa) using the soil type (predominant texture). The procedure consisted in selecting the mean values of θ_s and θ_r proposed in the tables obtained from those pedotransfer functions (Hodnett and Tomasella, 2002) for the predominant soil type of each geological unit, and fitting the α_G parameter to the curves with the same water content values but also with the fitting parameters (denoted as α_{vG} and n) that represents the soil type according to the van Genuchten's model (for those PTFs). The scarcity of measured data provides uncertainty in the results, but we consider that the implementation of the infiltration model for unsaturated soils provides more accurate slope stability results than the saturated model (Baum et al., 2010) even though simplifications were required defining some input parameters..

4.4 Reconstruction of possible rainfall triggering landslide events

Two landslide inventories (DesInventar, 2021; SIMMA, 2021) with historical records from the Valle de Aburrá region, between 1921 and 2017, were available. The inventories form the basis of a landslide database by AMVA and UNAL (2018). Out of the total 2,345 landslides in the inventory, only 1,533 could be considered in this research for the Medellín area; the others were labeled as having "high uncertainty". Uncertainty is due to unknown location: only the neighborhood, zone, or the city was recorded in the inventory. The scarce of accurate data from the landslide records was evident in the inventories. The unknown failure mechanism (*e.g.*, triggered by rainfall or anthropogenic activities) made it impossible to reconstruct more than a few (15) rainfall intensity and duration events that triggered landslides.

Historical rainfall records from rain gauges from EPM (Empresas Públicas de Medellín) in this region were used to extract the historical shallow landslide events that occurred within a radius of 3 km from the rain gauges. From seven rain gauges for which landslides closer than 3 km were found, only 13 landslides had rainfall records for the day or the day before the landslide date. For all of them, two or more watersheds were defined (varying the size of the drainage area between 0 and 2 km^2), and the methodologies for rainfall threshold definition were applied. Three of the rain gauges, Gerona (RG1), Planta Villa Hermosa (RG2) and San Antonio de Prado (RG3), and six watersheds were selected to compare the methodologies to define the thresholds and the rainfall events. The others were not considered since most of the associated rainfall events did not appear to be the triggering factor of the landslides due to their low mean intensities (<10-15 mm/h) and short durations (<1-3 h). Fig. 5 shows the location of six watersheds, including one watershed (W6) within the other (W5) and the three rain gauges. Table 5 shows the date of the landslides in watersheds from the Medellín study area. Fig. 6 shows the geological units of the watersheds.

5. Results

In this section, we describe the results obtained for the three study areas in three separate paragraphs.

5.1 La Arenosa basin

Fig. 7 shows the rainfall *I-D* thresholds for the La Arenosa basin using method M1 (*cfr*. Section 4.2), for different values of critical failure area, a_c: 0.1%, 1%, 3%, 5%, 10% and 20%. The *I-D* threshold curves are higher for increasing a_c. It is expected since more extreme rainfalls are required to cause more widespread slope instabilities. The figure also shows variations of the mean intensities during the shallow landslide triggering rainfall event on September 21st, 1990 (considered for this study area). We consider that different rainstorm subintervals represent different warning levels since the mean intensity varies for their specific durations. Fig. 7 shows that rainfall exceeded all of the thresholds during the storm. Furthermore, the events corresponding to the 2nd and 3rd hour of the rainstorm, and the point marked for only the third hour, exceed a few thresholds.

Fig. 8 shows the rainfall thresholds for the La Arenosa basin's grid cells, obtained with method M2. The maps of Fig. 8a and Fig. 8b represent values of the power-law parameters in Eq. (5) and its linearized version, Eq. (6). Fig. 8c is the initial duration for which the threshold is applicable (in hours). Fig. 8d is a map showing the factor of safety calculated in a scenario of completely saturated soil. The factor of safety maps in the completely saturated soil scenario correspond only to the most critical condition and it is presented to show which grid cells have a threshold (because they can fail) and which ones do not (because cannot fail due to any rainfall event). Fig. 8 only shows the grid cells for which a threshold could be obtained, *i.e.*, F_S was smaller than unity at some time during the storm. Almost one-half of the basin's grid cells could be associated with a threshold (49.2% of the total area). The scale parameter α varied mainly between 50 and 100 (53.8% of the total). Lower α values indicated lower thresholds, *i.e.*, less extreme rainfall events are required to cause instability. We found a marked tendency to decrease the shape parameter β as α increased.

We obtained thresholds for 2,042 of the grid cells from the landslide scarps inventory (93.1%). Fig. 9 shows 200 of these grid cells' threshold curves, selected at random, together with the intensity curves from the September 21st/1990 rainfall triggering event. The thresholds for grid cells were below the intensity curves (rainfall event) and corresponded with the shallow landslide occurrence due to the intense rainfall events. Out of 200 threshold curves that we considered, 62 (31%) predicted shallow landslide occurrence related to the last (3rd) hour of the rainfall event, with an average intensity of 90 mm/h (D = 1 h). This extreme intensity was considerably higher than the critical intensity of those 62 threshold curves with intensities varying between 65.6 mm/h and 24.2 mm/h (for D = 1 h). Within the whole event, landslide occurrence was predicted in 45 (22.5%) of the grid cells; and for the event including only the last two hours, landslides were predicted in 51 (25.5%) grid cells (with D = 1 h). The number of threshold curves below the rainfall event (predicting shallow landslide occurrence) increased for the second and third hours of the September 21st/1990 rainfall event..

Similarities in the threshold position using method M1 (Fig. 7) and method M2 (Fig. 9) were found, mostly in the lower curves. Still, differences from the end durations and the many curves related to each grid cell (using method M2) were expected. Many other thresholds, both for the grid cells with landslide scarps and over the rest of the basin, could be included or particularly analyzed in the duration-intensity graph shown in Fig. 9.

5.2 La Liboriana basin

Fig. 10 presents the rainfall *I-D* thresholds for the La Liboriana basin using method M1, Fig. 10(a), for different a_c values (0.1%, 1%, 3%, 5%, 10% and 20%), and method M2,

Fig. 10(b), for the 240 grid cells that were part of a landslide scarp in the landslide inventory (Fig. 4) and that have a threshold.

The variation of the mean intensities (in the high part of the basin) during the landslide triggering rainfall event on May 18th, 2015, is shown in Fig. 10. The thresholds are relatively low (even for the largest a_c values) compared with the obtained in the La Arenosa basin, mostly for short rainfall durations. This behavior was expected since very conservative soil strength parameters were selected in the simulations in this data-scarce study case. In this case, a more significant difference is evident for warning levels between the complete rainfall event and a part of it where the most extreme rainfall conditions occurred.

Fig. 11 presents the maps of the power-law parameters (α and β) that constitutes the threshold equation Eq. (6), in Fig. 11(a) and Fig. 11(b) respectively, the initial duration, Fig. 11(c), and the F_S map for a completely saturated soil scenario, Fig. 11(d), in the northern part (with higher elevations) of the basin.

5.3 Medellín area

We first calculated thresholds, using the same procedures for the La Arenosa and La Liboriana basins; *cfr* paragraphs 4.2 and 4.3, respectively. Fig. 12 shows the *I-D* thresholds for four watersheds (W1, W2, W3 and W4) from the Medellín area. The figure shows the results obtained using method M1 (W1, Fig. 12a; W2, Fig. 12c; W3, Fig. 12e; W4, Fig. 12g) for different a_c values, and method M2 (W1, Fig. 12b; W2, Fig. 12d; W3, Fig. 12f; W4, Fig. 12h) for all of the grid cells for which a threshold was obtained (except for W4, in which approximately one-half of the thresholds were charted). We found different thresholds in the different watersheds and different thresholds in the same watershed using methods M1 and M2, even though the curves appear to be very similar. We did not graph these thresholds in log-log axes as for the previous basins.

We further compared measured rainfall events with the thresholds were obtained by searching rainfall records from rain gauges closer than 3 km from the location of observed shallow landslides, described by the landslide inventories of Valle de Aburrá available to us. Results show that the only watershed with thresholds lower than one of the associated rainfall events was W1. A very clear separation between some of the thresholds was seen in this watershed (W1), with a less marked separation (between thresholds) in the others. The implementation of both methods helped to understand this behavior better.

Method M1 showed significant separation between the threshold curves of 0.3% and 0.5%. It was clarified understanding the curves' behavior in method M2 where each threshold (for each grid cell) has its specific location according to its physical properties (e.g., slope gradient and soil properties). As the thresholds with a percentage lower than 0.5% (of the grid cells) were located closer to the rainfall events (Fig. 12a, b) and the rest were so distant, then the curves from method M1 showed the same behavior. In other words, the threshold of 0.5% was reached only when the failure occurred in an additional grid cell. It was verified in the threshold curve location for specific grid cells (Fig. 12b, M2).

The maximum a_c included for the watersheds varied (M1, Fig. 12a, c, e, g) according to the maximum percentage of failing area. The very few numbers of grid cells (12) with a threshold (that were able to fail) in W2 represented only 0.16% of the watershed's total number of grid cells. On the other hand, W4 had 404 grid cells with a threshold (9.7% of the total) even though the watershed area is lower than W2.

Fig. 13 shows the maps of the power-law parameters, *i.e.*, the *I-D* thresholds using method M2, for each cell of the watershed W1. The figure's curves correspond to the same 27 grid cells with thresholds (2.1% of the basin) presented in Fig. 12b. The noticeable contrasts between the lower curves (lower α and/or higher β) and the others allow us to identify their location in the basin (map). All the grid cells with lower threshold curves have α parameters lower than 35 (Fig. 13(a)), and only those thresholds have an initial duration of 1 h (Fig. 13(c)).

Fig. 14 shows the *I-D* thresholds for two watersheds (W5 and W6) of San Antonio de Prado (district of Medellín). W6 is within W5. As in previous cases, the results correspond to thresholds defined using method M1, in Fig. 14(a) for W5 and Fig. 14(c) for W6, and method M2, for all of the grid cells with a threshold from W5, Fig. 14(b), and W6, Fig. 14(d).

All of the threshold curves for individual grid cells in W6, Fig. 14(d), are also in the ones of W5, Fig. 14(b). One can visually check that both watersheds' thresholds are very similar to the one from method M1. The expected additional curves from W5 (from method M2) are located in the upper part of Fig. 14(b). The lower threshold curves are relatively close to the curve representing the rainfall event associated with an observed shallow landslide in the study area.

Fig. 15 shows the thresholds for grid cells, represented in maps of the power-law parameters of Eqs. (5) and (6), using method M2 for the watershed W5 (including the thresholds for W6, as it is within W5). It elucidates again that the thresholds with lower α (producing a larger β) were the lower curves. The additional grid cells from W5, Fig. 14(b), have significantly higher α values than those of lower thresholds. It is the main reason we found no significant variation for thresholds using method M1 in both watersheds: the lower thresholds for the grid cells are almost the same. Hence, the failing area has little variation when the number of failing grid cells increases. If the failure of grid cells from W5 that are not the same as from W6, failure would occur with less extreme rainfall conditions. Thus the thresholds could not coincide (or be so similar) as compared with method M1.

6. Discussion

The use of physically-based models is an alternative approach to the typical calibration of rainfall thresholds on accurate knowledge of rainfall events that triggered landslides. Various approaches have been presented in the literature to deal with the lack of data to model landslide occurrence, including machine learning techniques (e.g., Generative Adversarial Networks, GANs), heuristic and statistical susceptibility models (Al-Najjar and Pradhan, 2021; Du et al., 2020; Lee et al., 2018; Jacobs et al., 2020), and with TRIGRS (Gioia et al., 2016; Marin et al., 2021b; Weidner et al., 2018).

Specifically, using TRIGRS to prepare rainfall *I-D* thresholds for shallow landslides is a promising tool to improve or complement statistical methods. The use of statistical methods for small or data-scarce areas is often impossible due to the sparse character of accurate data about rainfall data and landslide location. We devised two different methods for such a purpose; method M1 is defined at the (small) catchment scale, and method M2 is defined in individual grid cells. Thus, using method M1, thresholds depend on the entire study area, while using method M2, they are only influenced by local properties.

In this work, we validated physically-based thresholds by comparison with real rainfall events that triggered shallow landslides, at variance with previous implementations of both methods (Marin, 2020; Marin et al., 2020; Marin and Velásquez, 2020), in which validation was absent. We acknowledge that the comparison is not equivalent to a complete predictive performance evaluation, for which sufficient historical landslide and rainfall data would be needed.

Antecedent rainfall conditions of the events in the La Arenosa and La Liboriana basins were incorporated in a simplistic way using the I_{ZLT} input parameter of the TRIGRS model. I_{ZLT} is defined as the antecedent mean precipitation (generally related to recent weeks or few months) required to produce the steady infiltration rate previous the rainfall event (Baum et al., 2010). Variation of this parameter have an effect on the rainfall threshold position (Marin and Velásquez, 2020). Still, initial pore water pressures or groundwater levels were not assessed deeply due to lack of sufficient data and because it was not an objective of this study. Inclusion of antecedent conditions (or monitored pore water pressures) and definition thresholds for different antecedent scenarios in a specific study site is another valuable possibility of physically-based modeling.

The methods implemented in this research study (M1 and M2) differ in their applicability but can be complementary methods to provide a complete landslide assessment. The thresholds graphed using method M1 are of the kind of approaches (e.g., Papa et al. 2014, Alvioli et al., 2014) that constitute a selection of thresholds for a predefined percent failure area. It indicates that an appropriate application for M1 could be debris flow prediction because they usually occur when an extreme rainfall event causes multiple (clusters of) shallow landslides in a drainage basin, as occurred in the two catastrophic events that we studied (La Arenosa and La Liboriana basins)..

The thresholds obtained using method M2 differ from M1 in that the threshold curve is given to specific grid cells and that the spatial representation of the thresholds is shown in maps of the equation parameters (Eq. (5)). A graphical representation of the parameters in the thresholds gives an idea of the differences at grid cell level. Additional maps could include critical intensities for specific rainfall durations (e.g. 5 or 10 h) based on the power law-equation (presented in the maps of α, β, D_i and D_f). The usefulness of those thresholds is that specific portions of terrain (represented by grid cells) can be monitored in terms of the rainfall conditions that could cause a landslide that small area. Real-time rainfall events (spatially distributed or not) can generate alert (or advisory) levels for different interest areas at local scales (e.g. an infrastructure area or single slope).

Distributed thresholds have been less explored in the literature, but some approaches (Salciarini et al., 2012; Salciarini and Tamagnini, 2015) have provided spatially distributed critical intensities for specific rainfall durations. The distributed thresholds using M2 provide the specific slope's location for which its particular equation is applicable (for shallow landslide occurrence). Awareness about these thresholds' potential uncertainty is required since implementations of these methodologies often have entailed a not insignificant proportion of false alarms. It is natural since these models' applicability in the regional scale usually focuses on identifying potentially unstable areas more than a very detailed analysis of specific slopes' failure mechanisms. In this sense, the thresholds using M2 should be weighted with their uncertainty degree derived from the soil properties' description. Even a more detailed landslide modeling (Chen et al., 2021; Liu and Wang, 2021) can be used to improve the threshold accuracy. For example, a distributed approach was done by He et al. (2021), combining TRIGRS with the Scoops3D model. However, they defined a different kind of threshold (relating the instability proportion with the cumulative rainfall).

This uncertainty in the spatial prediction using method M2 exposes the importance of the availability of accurate input data (e.g., soil properties, topography) to obtain more accurate thresholds. It is probably more critical than using method M1 because the shallow landslides' specific location is not predicted in M1. Nevertheless, the accuracy of input data using physically based models is extensively acknowledged (Depina et al., 2020; Guzzetti et al., 2020; Keles and Nefeslioglu, 2021; Liang et al., 2021) and is pivotal to obtain satisfactory results using both methods.

For validation, the scarce availability of the landslide and triggering rainfall data was also a significant limitation for assessing the predictability of methods M1 and M2. The triggering rainfall events for our study cases required at least an hourly resolution but the greater challenge (and very common in other research studies) was to correctly associate rainfall triggering events to landslides recorded in existent inventories (for which there is no such specification). In our research study, the rainfall events associated with the landslide records from Medellín have a high degree of uncertainty in the time of the event (the same and the past day were considered) and the amount of rainfall (location of the rain gauges: <3 km). Since a specific triggering rainfall event was not the input data for the rainfall threshold definition (in the methods), the uncertainty applies to the thresholds' comparison or validation.

7. Conclusions

We suggested the application of TRIGRS, a time-dependent, distributed model for slope stability assessment for defining rainfall intensity and duration thresholds in three study areas from the Colombian Andes. Like many slope distributed stability models, the main output of TRIGRS is an F_S grid. Rainfall thresholds are not among the outputs of the model.

Thus, the definition of rainfall thresholds required devising sound methods to link the model's input rainfall to the output grid.

Two physically-based methodologies (M1 and M2) to define rainfall thresholds for shallow landslides potentially constitute good tools for landslide early warning systems. Understanding the differences between the two kinds of thresholds and possible independent applicability (method M1 can be a tool for debris flow prediction and method M2 can provide a more accurate specification of landslide source locations) will help select the more appropriate method, and the two methods can be complementary. As the validation of the rainfall thresholds before its implementation in a LEWS is very important, the comparison between rainfall triggering events and thresholds defined with both methods applied in the Colombian Andes is valuable to assess their predictive performance. The limitations for evaluating the thresholds' predictive capacity highlight the need to improve the accuracy of landslide records in the area.

Future studies, not only in mountain terrains of Colombia but all over the world, could be focused on validating the physically-based thresholds of methods M1 and M2 using sophisticated approaches to incorporate successes and false alarms, according to different soil moisture conditions, including historical rainfall that caused and did not cause shallow landslides (e.g., ROC analysis) in the specific watersheds or hillslopes. Probabilistic approaches to incorporate the uncertainty in the analysis is another challenge for these kinds of thresholds.

Acknowledgements: This work was supported by Landslide Scientific Assessment (LandScient), Universidad de Antioquia, and Grupo de Investigación en Infraestructura (GII).

References

Al-Najjar, H.A.H., Pradhan, B., 2021. Spatial landslide susceptibility assessment using machine learning techniques assisted by additional data created with generative adversarial networks. Geosci. Front. 12, 625–637. https://doi.org/10.1016/j.gsf.2020.09.002

Alvioli, M., Baum, R.L., 2016. Parallelization of the TRIGRS model for rainfall-induced landslides using the message passing interface. Environ. Model. Softw. 81, 122–135. https://doi.org/10.1016/j.envsoft.2016.04.002

Alvioli, M., Guzzetti, F., Rossi, M., 2014. Scaling properties of rainfall induced landslides predicted by a physically based model. Geomorphology 213, 38–47. https://doi.org/10.1016/j.geomorph.2013.12.039

Alvioli, M., Melillo, M., Guzzetti, F., Rossi, M., Palazzi, E., von Hardenberg, J., Brunetti, M.T., Peruccacci, S., 2018. Implications of climate change on landslide hazard in Central Italy. Sci. Total Environ. 630, 1528–1543. https://doi.org/10.1016/j.scitotenv.2018.02.315

AMVA, 2016. Armonización de la microzonificación sísmica de los municipios del Valle de Aburrá, al reglamento NSR-10 e inclusión de los cinco corregimientos del

Municipio de Medellín.
AMVA, UNAL, 2018. Estudios básicos de amenaza por movimientos en masa, inundaciones y avenidas torrenciales en los municipios de Caldas, La Estrella, Envigado, Itagüí, Bello, Copacabana y Barbosa, para la incorporación de la gestión del riesgo en la planificación territorial. Área Metropolitana del Valle del Aburrá, Medellín.
Aristizábal, E., Roser, B., Yokota, S., 2005. Tropical chemical weathering of hillslope deposits and bedrock source in the Valle de Aburrá, northern Colombian Andes. Eng. Geol. 81, 389–406. https://doi.org/https://doi.org/10.1016/j.enggeo.2005.08.001
Aristizábal, E., 2013. SHIA_Landslide: Developing a physically based model to predict shallow landslides triggered by rainfall in tropical environments. Ph Thesis, Univ. Nac. Colomb.
Aristizábal, E., García, E., Martínez, C., 2015. Susceptibility assessment of shallow landslides triggered by rainfall in tropical basins and mountainous terrains. Nat. Hazards 78, 621–634.
Aristizábal, E., Vélez, J.I., Martínez, H.E., Jaboyedoff, M., 2016. SHIA_Landslide: a distributed conceptual and physically based model to forecast the temporal and spatial occurrence of shallow landslides triggered by rainfall in tropical and mountainous basins. Landslides 13, 497–517. https://doi.org/10.1007/s10346-015-0580-7
ASF: Dataset: ASF DAAC 2015. ALOS PALSAR – Radiometric Terrain Correction. Includes Material© JAXA/METI, 2007. Accessed through ASF DAAC 2019. https://doi.org/10.5067/Z97HFCNKR6VA
Baum, R.L., Godt, J.W., Savage, W.Z., 2010. Estimating the timing and location of shallow rainfall-induced landslides using a model for transient, unsaturated infiltration. Journal of Geophysical Research: Earth Surface, 115(F3).
Baum, R.L., Savage, W.Z., Godt, J.W., 2008. TRIGRS- A Fortran Program for Transient Rainfall Infiltration and Grid-Based Regional Slope-Stability Analysis, Version 2. 0. U. S. Geological Survey.
Baum, R.L., Savage, W.Z., Godt, J.W., 2002. TRIGRS–a Fortran program for transient rainfall infiltration and grid-based regional slope-stability analysis. USGS Open-File Report 02–0424. US Geol. Surv. Reston, VA.
Baumann, V., Bonadonna, C., Cuomo, S., Moscariello, M., Manzella, I., 2018. Slope stability models for rainfall-induced lahars during long-lasting eruptions. J. Volcanol. Geotherm. Res. 359, 78–94. https://doi.org/10.1016/j.jvolgeores.2018.06.018
Bordoni, M., Corradini, B., Lucchelli, L., Valentino, R., Bittelli, M., Vivaldi, V., Meisina, C., 2019. Empirical and Physically Based Thresholds for the Occurrence of Shallow Landslides in a Prone Area of Northern Italian Apennines. Water 11, 2653. https://doi.org/10.3390/w11122653
Brunetti, M.T., Peruccacci, S., Rossi, M., Luciani, S., Valigi, D., Guzzetti, F., 2010. Rainfall thresholds for the possible occurrence of landslides in Italy. Natural Hazards and Earth System Sciences 10 (3), 447-458. https://doi.org/10.5194/nhess-10-447-2010

Budhu, M., 2015. Soil mechanics fundamentals. John Wiley & Sons.

Chatra, A.S., Dodagoudar, G.R., Maji, V.B., 2019. Numerical modelling of rainfall effects on the stability of soil slopes. Int. J. Geotech. Eng. 13, 425–437. https://doi.org/10.1080/19386362.2017.1359912

Chen, X., Zhang, Lulu, Zhang, Limin, Zhou, Y., Ye, G., Guo, N., 2021. Modelling rainfall-induced landslides from initiation of instability to post-failure. Comput. Geotech. 129, 103877. https://doi.org/10.1016/j.compgeo.2020.103877

Chowdhury, R., 2010. Geotechnical Slope Analysis, Engineering and Science. https://doi.org/10.1201/9780203864203

Ciurleo, M., Mandaglio, M.C., Moraci, N., 2019. Landslide susceptibility assessment by TRIGRS in a frequently affected shallow instability area. Landslides 16, 175–188. https://doi.org/10.1007/s10346-018-1072-3

Das, B.M., 2013. Advanced Soil Mechanics. CRC Press.

Dearman, W.R., 1991. Engineering Geological Mapping. Elsevier. https://doi.org/10.1016/C2013-0-01209-1

Depina, I., Oguz, E.A., Thakur, V., 2020. Novel Bayesian framework for calibration of spatially distributed physical-based landslide prediction models. Comput. Geotech. 125, 103660. https://doi.org/10.1016/j.compgeo.2020.103660

DesInventar, 2021. Sistema de inventarios de efectos de desastres [WWW Document]. URL https://www.desinventar.org/

Du, J., Glade, T., Woldai, T., Chai, B., Zeng, B., 2020. Landslide susceptibility assessment based on an incomplete landslide inventory in the Jilong Valley, Tibet, Chinese Himalayas. Eng. Geol. 270, 105572. https://doi.org/10.1016/j.enggeo.2020.105572

Ewen, J., Parkin, G., O'Connell, P.E., 2000. SHETRAN: Distributed River Basin Flow and Transport Modeling System. J. Hydrol. Eng. 5, 250–258. https://doi.org/10.1061/(ASCE)1084-0699(2000)5:3(250)

Fusco, De Vita, Mirus, Baum, Allocca, Tufano, Di Clemente, Calcaterra, 2019. Physically Based Estimation of Rainfall Thresholds Triggering Shallow Landslides in Volcanic Slopes of Southern Italy. Water 11, 1915. https://doi.org/10.3390/w11091915

Gardner, W.R., 1958. Some steady-state solutions of the unsaturated moisture flow equation with application to evaporation from a water table. Soil Sci. 85, 228–232. https://doi.org/10.1097/00010694-195804000-00006

Ghanbarian, B., Hunt, A.G., 2017. Improving unsaturated hydraulic conductivity estimation in soils via percolation theory. Geoderma 303, 9–18

Gioia, E., Speranza, G., Ferretti, M., Godt, J.W., Baum, R.L., Marincioni, F., 2016. Application of a process-based shallow landslide hazard model over a broad area in Central Italy. Landslides 13, 1197–1214. https://doi.org/10.1007/s10346-015-0670-6

Grima, N., Edwards, D., Edwards, F., Petley, D., Fisher, B., 2020. Landslides in the Andes: Forests can provide cost-effective landslide regulation services. Sci. Total Environ. 745, 141128. https://doi.org/10.1016/j.scitotenv.2020.141128

Guzzetti, F., Gariano, S.L., Peruccacci, S., Brunetti, M.T., Marchesini, I., Rossi, M., Melillo, M., 2020. Geographical landslide early warning systems. Earth-Science Rev. 200, 102973. https://doi.org/10.1016/j.earscirev.2019.102973

Guzzetti, F., Peruccacci, S., Rossi, M., Stark, C.P., 2008. The rainfall intensity–duration control of shallow landslides and debris flows: an update. Landslides 5, 3–17. https://doi.org/10.1007/s10346-007-0112-1

He, J., Qiu, H., Qu, F., Hu, S., Yang, D., Shen, Y., Zhang, Y., Sun, H., Cao, M., 2021. Prediction of spatiotemporal stability and rainfall threshold of shallow landslides using the TRIGRS and Scoops3D models. CATENA 197, 104999. https://doi.org/10.1016/j.catena.2020.104999

Hodnett, M.G., Tomasella, J., 2002. Marked differences between van Genuchten soil water-retention parameters for temperate and tropical soils: a new water-retention pedo-transfer functions developed for tropical soils. Geoderma 108, 155–180. https://doi.org/10.1016/S0016-7061(02)00105-2

Huang, Y.H., 2012. Stability analysis of earth slopes. Springer Science & Business Media

INTEGRAL, S.A., 1990. Informe sobre daños en la central de calderas por la avalancha ocurrida en l quebrada LA Arenosa el 21 de septiembre de 1990 y su reparación. Interconexión eléctrica SA (ISA), Medellín, Colomb. Rep.

Intrieri, E., Gigli, G., Casagli, N., Nadim, F., 2013. Brief communication: Landslide Early Warning System: toolbox and general concepts. Nat. Hazards Earth Syst. Sci. 13, 85–90. https://doi.org/10.5194/nhess-13-85-2013

ISA, Integral, Cornare, Colombia, U. de, 1991. Proyecto Hidroelectrico de Calderas-Estudio de recuperación y manejo de la cuenca hidrográfica de la Quebrada La Arenosa, Vol 1. ed. Medellín: ISA.

Keles, F., Nefeslioglu, H.A., 2021. Infinite slope stability model and steady-state hydrology-based shallow landslide susceptibility evaluations: The Guneysu catchment area (Rize, Turkey). CATENA 200, 105161. https://doi.org/10.1016/j.catena.2021.105161

Jacobs, L., Kervyn, M., Reichenbach, P., Rossi, M., Marchesini, I., Alvioli, M., Dewitte, O., 2020. Regional susceptibility assessments with heterogeneous landslide information: Slope unit- vs. pixel-based approach. Geomorphology 356, 107084. https://doi.org/10.1016/j.geomorph.2020.107084

Lee, J.-H., Sameen, M.I., Pradhan, B., Park, H.-J., 2018. Modeling landslide susceptibility in data-scarce environments using optimized data mining and statistical methods. Geomorphology 303, 284–298. https://doi.org/10.1016/j.geomorph.2017.12.007

Liang, D., Hua, W., Liu, X., Zhao, Y., Liu, Z., 2021. Uncertainty assessment of a 3D geological model by integrating data errors, spatial variations and cognition bias. Earth Sci. Informatics 14, 161–178. https://doi.org/10.1007/s12145-020-00548-4

Liu, X., Wang, Y., 2021. Probabilistic simulation of entire process of rainfall-induced landslides using random finite element and material point methods with hydro-mechanical coupling. Comput. Geotech. 132, 103989. https://doi.org/10.1016/j.compgeo.2020.103989

Marin, R.J., 2020. Physically based and distributed rainfall intensity and duration thresholds for shallow landslides. Landslides 17, 2907–2917. https://doi.org/10.1007/s10346-020-01481-9

Marín, R.J., García-Aristizábal, E., Aristizábal, E., García, E., Aristizábal, E., 2019. Umbrales de lluvia para deslizamientos superficiales basados en modelos físicos: aplicación en una subcuenca del Valle de Aburrá (Colombia). DYNA 86, 312–322.

https://doi.org/10.15446/dyna.v86n210.77166

Marin, R.J., García, E.F., Aristizábal, E., 2020. Effect of basin morphometric parameters on physically-based rainfall thresholds for shallow landslides. Eng. Geol. 278, 105855. https://doi.org/10.1016/j.enggeo.2020.105855

Marin, R.J., Mattos, Á.J., 2020. Physically-based landslide susceptibility analysis using Monte Carlo simulation in a tropical mountain basin. Georisk Assess. Manag. Risk Eng. Syst. Geohazards 14, 192–205. https://doi.org/10.1080/17499518.2019.1633582

Marin, R.J., Velásquez, M.F., 2020. Influence of hydraulic properties on physically modelling slope stability and the definition of rainfall thresholds for shallow landslides. Geomorphology 351, 106976. https://doi.org/10.1016/j.geomorph.2019.106976

Marin, R.J., García, E.F., Aristizábal, E., 2021a. Assessing the Effectiveness of TRIGRS for Predicting Unstable Areas in a Tropical Mountain Basin (Colombian Andes). Geotech. Geol. Eng. https://doi.org/10.1007/s10706-020-01630-w

Marin, R.J., Velásquez, M.F., Sánchez, O., 2021b. Applicability and performance of deterministic and probabilistic physically based landslide modeling in a data-scarce environment of the Colombian Andes. J. South Am. Earth Sci. 108, 103175. https://doi.org/10.1016/j.jsames.2021.103175

Martínez-Carvajal, H.E., de Moraes Guimarães Silva, M.T., García-Aristizábal, E.F., Aristizábal-Giraldo, E. V, Larios-Benavides, M.A., 2018. A mathematical approach for assessing landslide vulnerability. Earth Sci. Res. J. 22, 251–273.

Mejía, R., Velásquez, M.E., 1991. Procesos y depósitos asociados al aguacero de septiembre 21 de 1990 en el Área de San Carlos (Antioquia). Undergrad. Thesis, Universidad Nacional de Colombia sede Medellín. Medellín.

Melillo, M., Gariano, S.L., Peruccacci, S., Sarro, R., Mateos, R.M., Brunetti, M.T. (2020). Rainfall and rockfalls in the Canary Islands: assessing a seasonal link. Natural Hazards and Earth System Sciences 20 (8), 2307-2317. https://doi.org/10.5194/nhess-20-2307-2020

Montrasio, L., Valentino, R., Losi, G.L., 2011. Towards a real-time susceptibility assessment of rainfall-induced shallow landslides on a regional scale. Nat. hazards earth Syst. Sci. 11, 1927.

Osorio, H.G., 2008. AS: Unidades de suelo representativas de la zona cafetera de Colombia. Fed. Cafe. 890.

Papa, M.N., Medina, V., Ciervo, F., Bateman, A., 2013. Derivation of critical rainfall thresholds for shallow landslides as a tool for debris flow early warning systems. Hydrol. Earth Syst. Sci. 17, 4095–4107. https://doi.org/10.5194/hess-17-4095-2013

Park, D.W., Nikhil, N. V, Lee, S.R., 2013. Landslide and debris flow susceptibility zonation using TRIGRS for the 2011 Seoul landslide event. Nat. Hazards Earth Syst. Sci. 13, 2833–2849.

Ramos-Cañón, A.M., Prada-Sarmiento, L.F., Trujillo-Vela, M.G., Macías, J.P., Santos-R, A.C., 2016. Linear discriminant analysis to describe the relationship between rainfall and landslides in Bogotá, Colombia. Landslides 13, 671–681. https://doi.org/10.1007/s10346-015-0593-2

Restrepo, J.J., Toussaint, J., 1984. Acreciones sucesivas en Colombia: Un nuevo modelo

de evolución geológica, in: I Conferencia de Riesgos Geológicos Del Valle de Aburrá. Medellín, p. 26.
Richards, L.A., 1931. Capillary conduction of liquids through porous mediums. Physics (College. Park. Md). 1, 318–333.
Ruiz Vásquez, D., 2017. Landslide susceptibility assessment in mountainous and tropical scarce-data regions using remote sensing data: a case study in the Colombian Andes. Undergrad. Thesis. Universidad EAFIT. Medellín.
Salciarini, D., Tamagnini, C., 2015. Physically–based critical rainfall thresholds for unsaturated soil slopes, in: Recent Advances in Modeling Landslides and Debris Flows. Springer, pp. 253–264.
Salciarini, D., Tamagnini, C., Conversini, P., Rapinesi, S., 2012. Spatially distributed rainfall thresholds for the initiation of shallow landslides. Nat. Hazards 61, 229–245. https://doi.org/10.1007/s11069-011-9739-2
Saulnier, G.-M., Beven, K., Obled, C., 1997. Including spatially variable effective soil depths in TOPMODEL. J. Hydrol. 202, 158–172. https://doi.org/10.1016/S0022-1694(97)00059-0
Segoni, S., Piciullo, L., Gariano, S.L., 2018. A review of the recent literature on rainfall thresholds for landslide occurrence. Landslides 15, 1483–1501. https://doi.org/10.1007/s10346-018-0966-4
SGC - Servicio Geológico Colombian, 2014. Memoria explicativa del mapa geomorfológico aplicado a movimientos en masa esc 1:100.000. plancha 166 - Jericó. Sogamoso.
SGC - Servicio Geológico Colombiano, 2014. Memoria explicativa del mapa geomorfológico aplicado a movimientos en masa esc 1:100.000. plancha 165 - Carmen de Atrato. Medellín.
SIMMA, 2021. Sistema de información de movimientos en masa. Colombia [WWW Document].
Taylor, D.W., 1948. Fundamentals of soil mechanics. Soil Sci. 66, 161.
Tran, T.V., Lee, G., Thu, T.M., An, H.U., 2017. Effect of Digital Elevation Model Resolution on Shallow Landslide Modeling Using TRIGRS. Nat. Hazards Rev. 18, 04016011. https://doi.org/10.1061/(ASCE)NH.1527-6996.0000233
Tran, T.V., Alvioli, M., Lee, G., An, H.U, 2018. Three-dimensional, time-dependent modeling of rainfall-induced landslides over a digital landscape: a case study. Landslides 15**,** 1071–1084. https://doi.org/10.1007/s10346-017-0931-7
Toussaint, J.F., Restrepo, J.J., 1994. The Colombian Andes During Cretaceous Times, in: Cretaceous Tectonics of the Andes. Vieweg+Teubner Verlag, Wiesbaden, pp. 61–100. https://doi.org/10.1007/978-3-322-85472-8_2
van Genuchten, M.T., 1980. A closed-form equation for predicting the hydraulic conductivity of unsaturated soils. Soil Sci. Soc. Am. J. 44, 892–898.
Vanapalli, S.K., Fredlund, D.G., 2000. Comparison of different procedures to predict unsaturated soil shear strength, in: Advances in Unsaturated Geotechnics. pp. 195–209.
Vega, J.A., Hidalgo, C.A., 2016. Quantitative risk assessment of landslides triggered by earthquakes and rainfall based on direct costs of urban buildings. Geomorphology

273, 217–235. https://doi.org/10.1016/j.geomorph.2016.07.032

Vessia, G., Di Curzio, D., Chiaudani, A., Rusi, S., 2020. Regional rainfall threshold maps drawn through multivariate geostatistical techniques for shallow landslide hazard zonation. Sci. Total Environ. 705, 135815. https://doi.org/10.1016/j.scitotenv.2019.135815

Weidner, L., Oommen, T., Escobar-Wolf, R., Sajinkumar, K.S., Samuel, R.A., 2018. Regional-scale back-analysis using TRIGRS: an approach to advance landslide hazard modeling and prediction in sparse data regions. Landslides 15, 2343–2356. https://doi.org/10.1007/s10346-018-1044-7

Zhao, B., Dai, Q., Han, D., Dai, H., Mao, J., Zhuo, L., 2019. Probabilistic thresholds for landslides warning by integrating soil moisture conditions with rainfall thresholds. J. Hydrol. 574, 276–287. https://doi.org/10.1016/j.jhydrol.2019.04.062

Zhao, B., Dai, Q., Han, D., Zhang, J., Zhuo, L., Berti, M., 2020. Application of hydrological model simulations in landslide predictions. Landslides 17, 877–891. https://doi.org/10.1007/s10346-019-01296-3

Table 1. Geotechnical and hydraulic soil parameters used in the model for each geological unit in the La Arenosa basin in San Carlos's municipality.

Parameter	c' [kN/m^2]	ϕ' [deg]	γ_s [kN/m^3]	K_s [m/s]	D_0 [m^2/s]	θ_s	θ_r	α_G [m^{-1}]
Alluvial soil	1.5	39.1	20	5.33×10^{-6}	5.33×10^{-4}	0.48	0.18	2.3
Residual soil	7.3	27.6	18	1.5×10^{-5}	1.5×10^{-3}	0.46	0.18	2.3

Table 2. Geotechnical and hydraulic soil parameters used in the model for each geological unit in the La Liboriana basin (Salgar).

Parameter	c' [kN/m^2]	ϕ' [deg]	γ_s [kN/m^3]	K_s [m/s]	D_0 [m^2/s]	θ_s	θ_r	α_G [m^{-1}]
Upper Cretaceous sedimentary rocks (Kaa)	10.5	24	19	1.39×10^{-5}	1.39×10^{-3}	0.519	0.226	1
Quaternary deposits (Qar)	18	30	17	1.4×10^{-8}	1.4×10^{-6}	0.46	0.18	1.4
Miocene intrusive igneous rocks (Tdt)	5	32	19.5	1.53×10^{-7}	1.53×10^{-5}	0.519	0.226	1

Table 3. Geotechnical and hydraulic soil parameters used in the model for each geological unit of the watersheds from Medellín.

Parameter	***c'*** [kN/m^2]	***φ'*** [deg]	***γ$_s$*** [kN/m^3]	***K$_s$*** [m/s]	***D$_0$*** [m^2/s]	**θ$_s$**	**θ$_r$**	***α$_G$*** [m^{-1}]
Amphibolites from Medellín (TRaM)	20	24	17.5	4.86×10^{-6}	4.86×10^{-4}	0.57	0.278	1.2
Alluvial-torrential deposits (Qat)	9.5	28.5	12	2.33×10^{-5}	2.33×10^{-3}	0.461	0.111	1.4
Recent landslide deposits (Qdr)	13	15	19.2	4.86×10^{-6}	4.86×10^{-4}	0.57	0.278	1.2
Debris/mud flow deposits (NFI)	18.5	20	17	1.01×10^{-5}	1.01×10^{-3}	0.601	0.223	1
Debris/mud flow deposits (NFpreI)	17.1	19.4	17.5	1.01×10^{-5}	1.01×10^{-3}	0.601	0.223	1
Debris/mud flow deposits (NQFII)	20	19	18.2	1.01×10^{-5}	1.01×10^{-3}	0.601	0.223	1
Debris/mud flow deposits (QFIII)	17.5	21	16.5	1.01×10^{-5}	1.01×10^{-3}	0.601	0.223	1
Debris/mud flow deposits (QFIV)	17	22	16.5	1.01×10^{-5}	1.01×10^{-3}	0.601	0.223	1
Dunite from Medellín (JKuM)	11.2	17.2	23	9.72×10^{-6}	9.72×10^{-4}	0.586	0.267	1.3
Anthropogenic fills (Qll)	10	33	11	2.06×10^{-5}	2.06×10^{-3}	0.41	0.037	2
Volcano-sedimentary member (KvsQG)	13.5	19	22	4.86×10^{-6}	4.86×10^{-4}	0.57	0.278	1.2
Stock from San Diego (KgSD)	14.3	21.5	13.6	1.13×10^{-5}	1.13×10^{-3}	0.601	0.223	1
Stock from Las Estancias (KcdE)	10.7	21.8	19.7	1.13×10^{-5}	1.13×10^{-3}	0.601	0.223	1

Table 4. Implemented ranges of durations for the definition of thresholds with varying steps of increments.

Time Step [h]	**Duration Range** [h]
1	1 - 10
2	10 - 30
3	30 - 60

Table 5. Date of the landslides in watersheds from Medellín.

Watershed	Location	Area [km^2]	Landslide date
W1	Medellín (East)	0.13	26/08/2008
W2	Medellín (East)	0.745	14/03/2003 13/11/2010
W3	Medellín (East)	0.978	28/03/2003
W4	Medellín (East)	0.415	28/03/2003
W5	Medellín (South-West), San Antonio de Prado	0.236	7/11/2001
W6	Medellín (South-West), San Antonio de Prado	0.186	7/11/2001

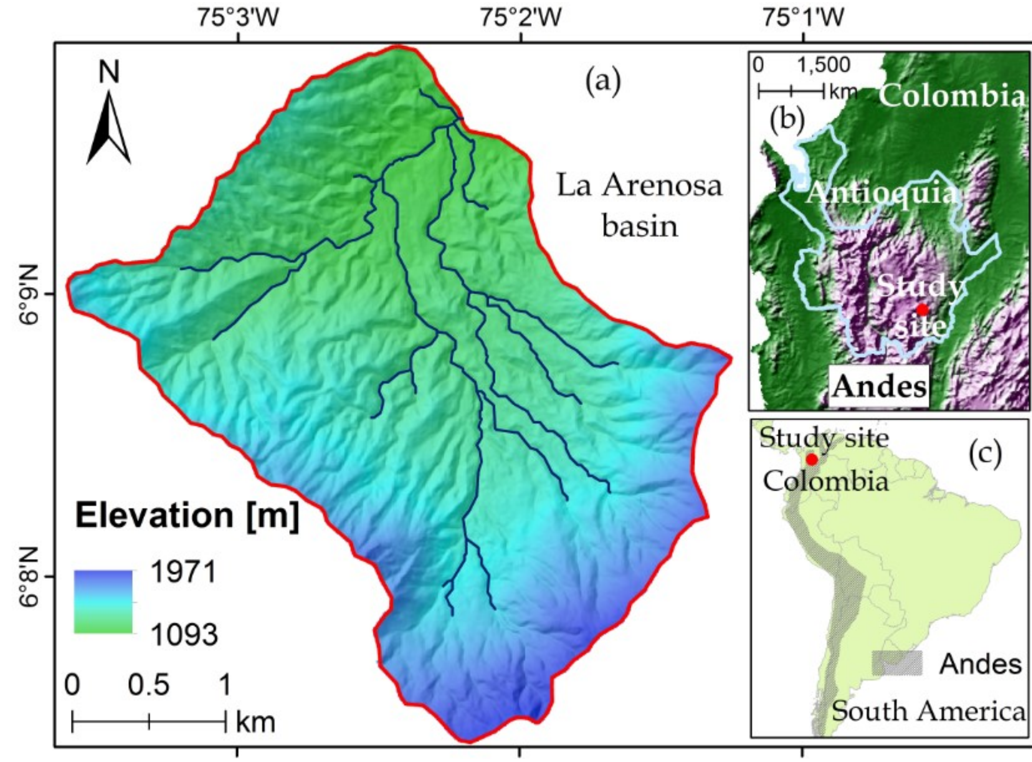

Fig. 1. Location of the La Arenosa basin (San Carlos, Colombia): (a) Digital elevation model (basin); (b) location in Antioquia, Colombia; (c) location in South America.

928

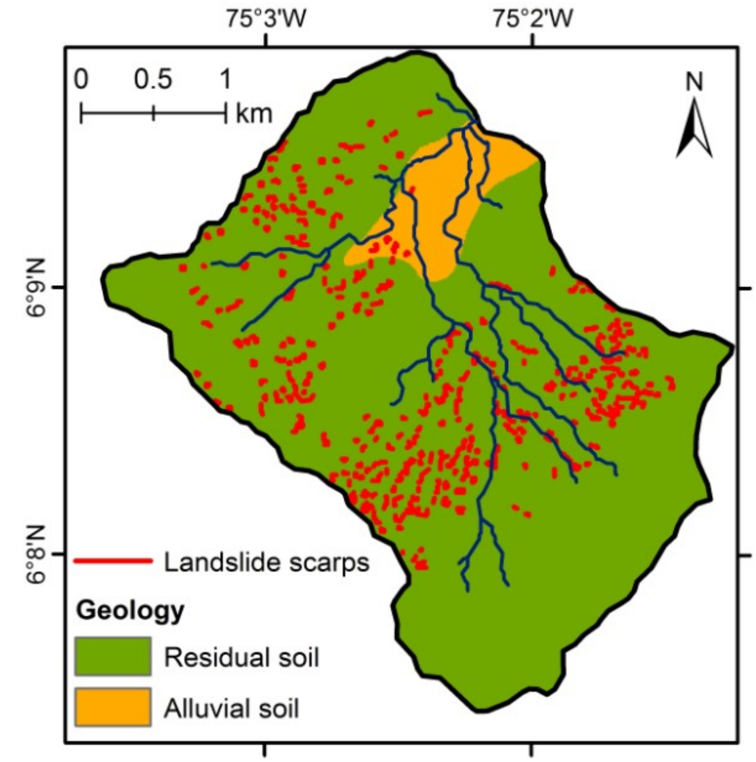

Fig. 2. Geology of the La Arenosa basin and landslide inventory (scarps) of the September 21st, 1990 event.

929

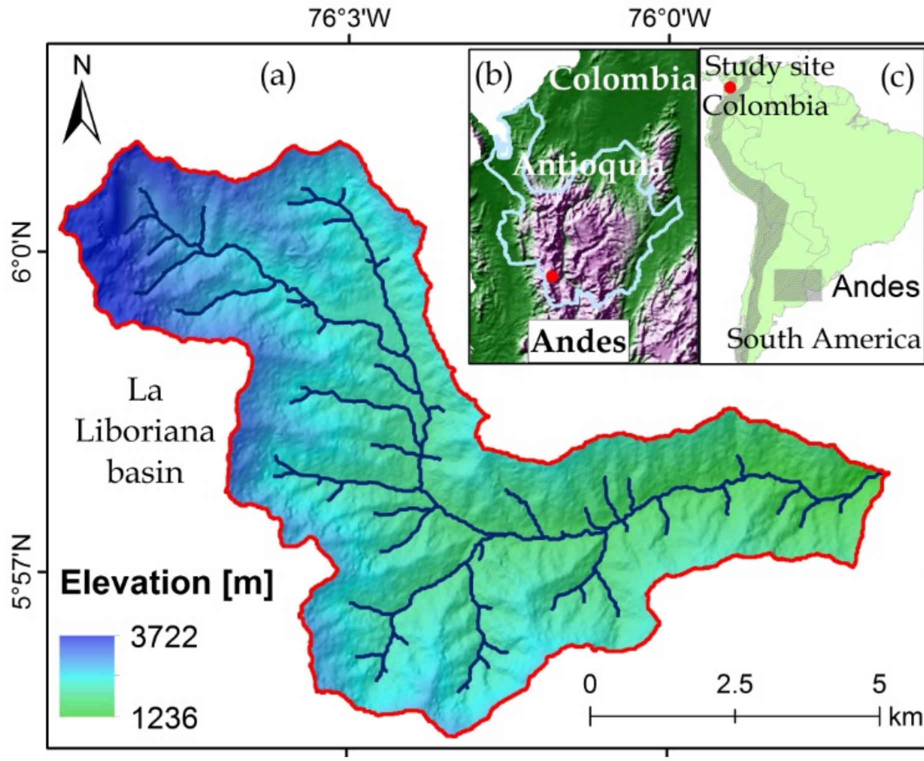

Fig. 3. Location of the La Liboriana basin (Salgar, Colombia): (a) Digital elevation model (basin); (b) location in Antioquia, Colombia; (c) location in South America.

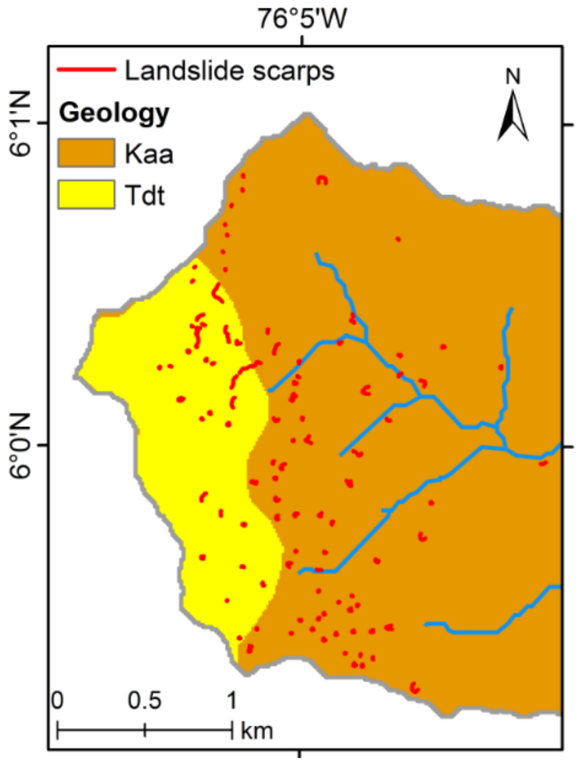

Fig. 4. Geology of the high part of the La Liboriana basin (Salgar, Colombia) and landslide inventory (scarps) (May 18th, 2015 landslide event).

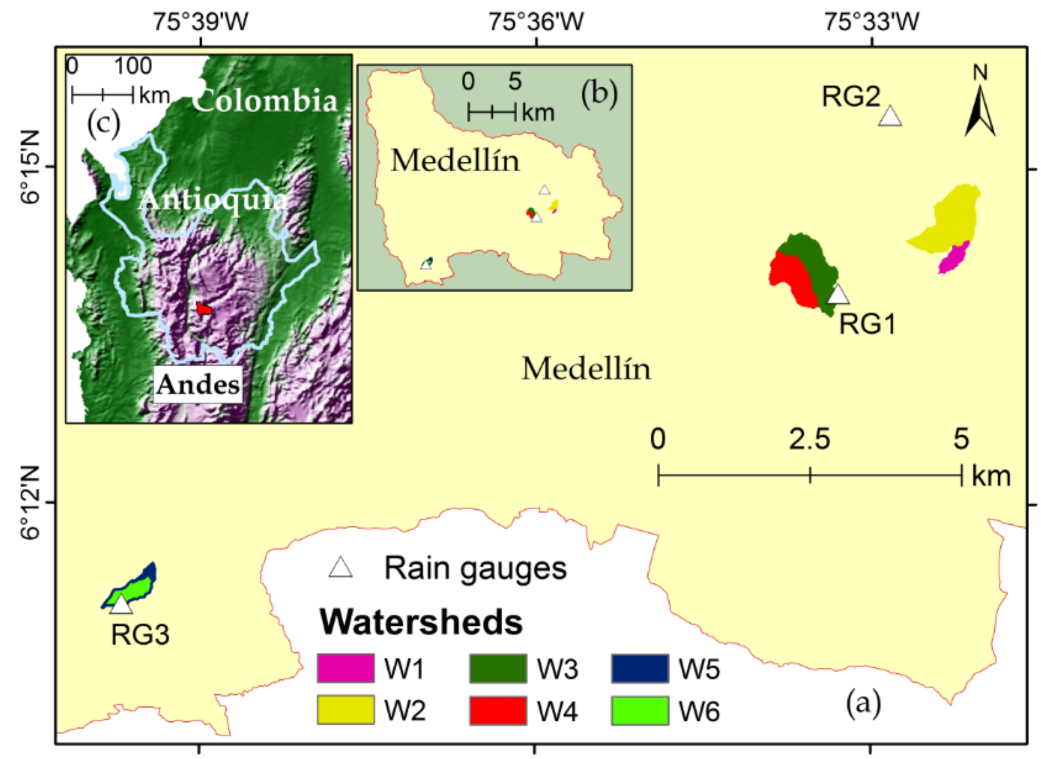

Fig. 5. Location of the (a) small watersheds (W1-W6) in the Medellín area and rain gauges (RG1-RG3); (b) location of the watersheds in Medellín; (c) location in Antioquia, Colombia.

934

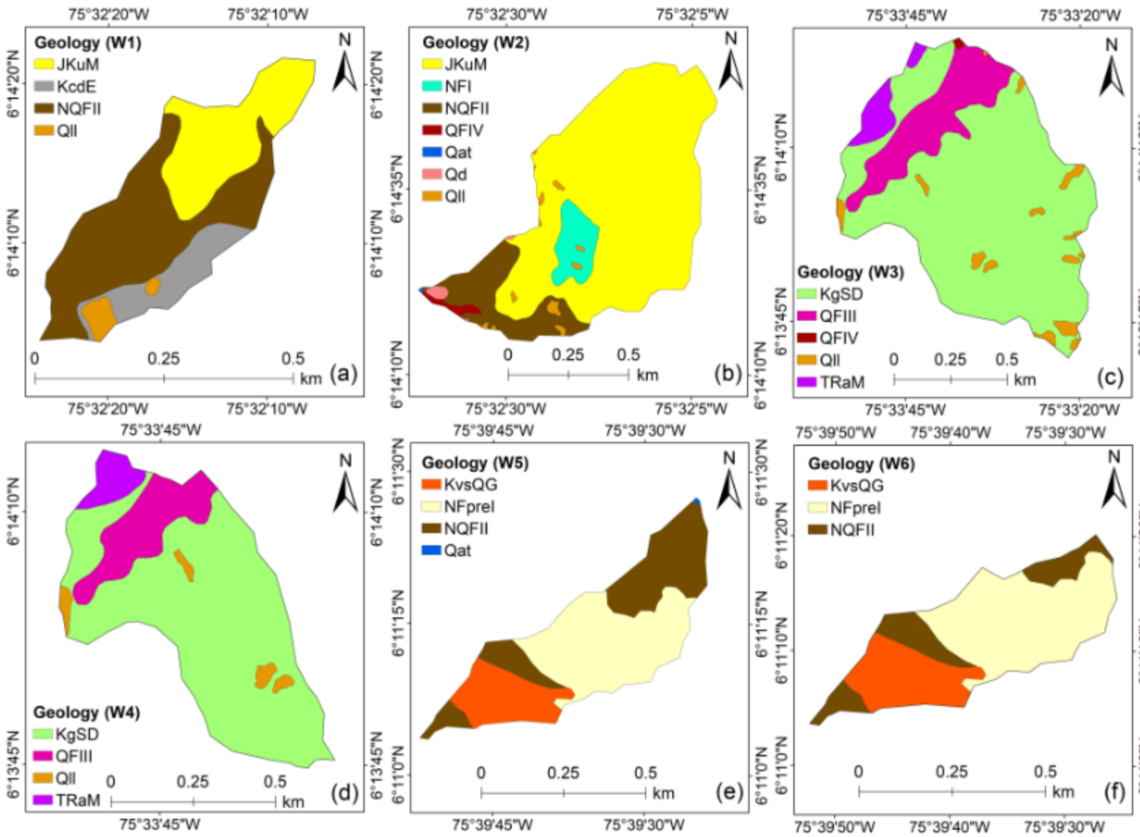

Fig. 6. Geology of the small watersheds of Medellín (W1-W6). Location of the watersheds is shown in Fig. 5. The names of geological units are listed in Table 3.

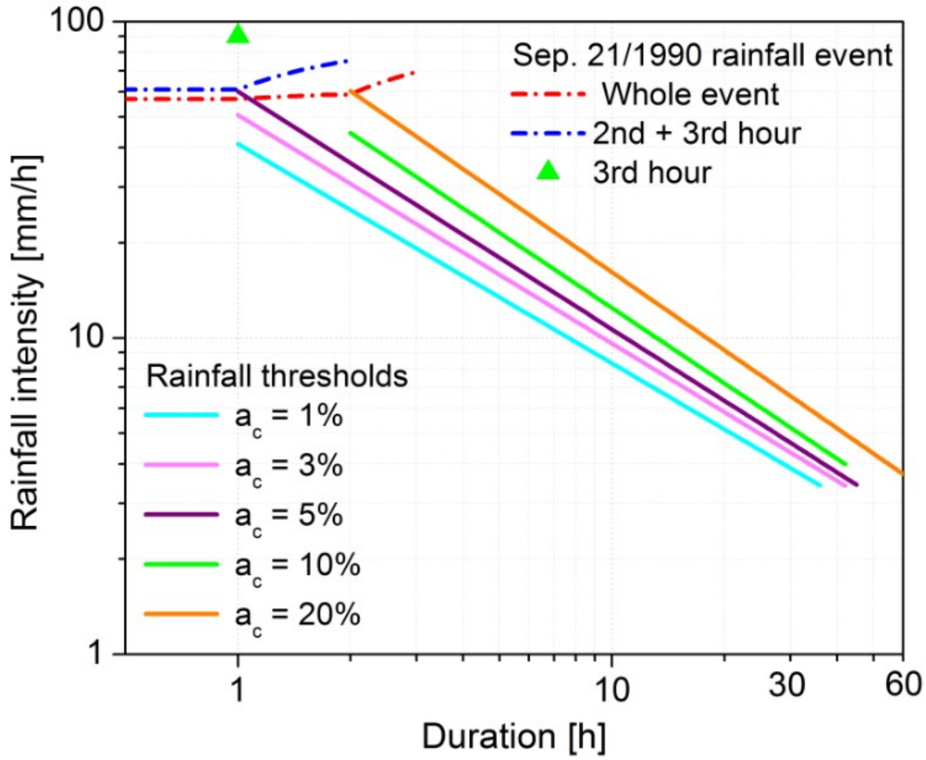

Fig. 7. Rainfall thresholds for the La Arenosa basin using method M1 for different a_c values.

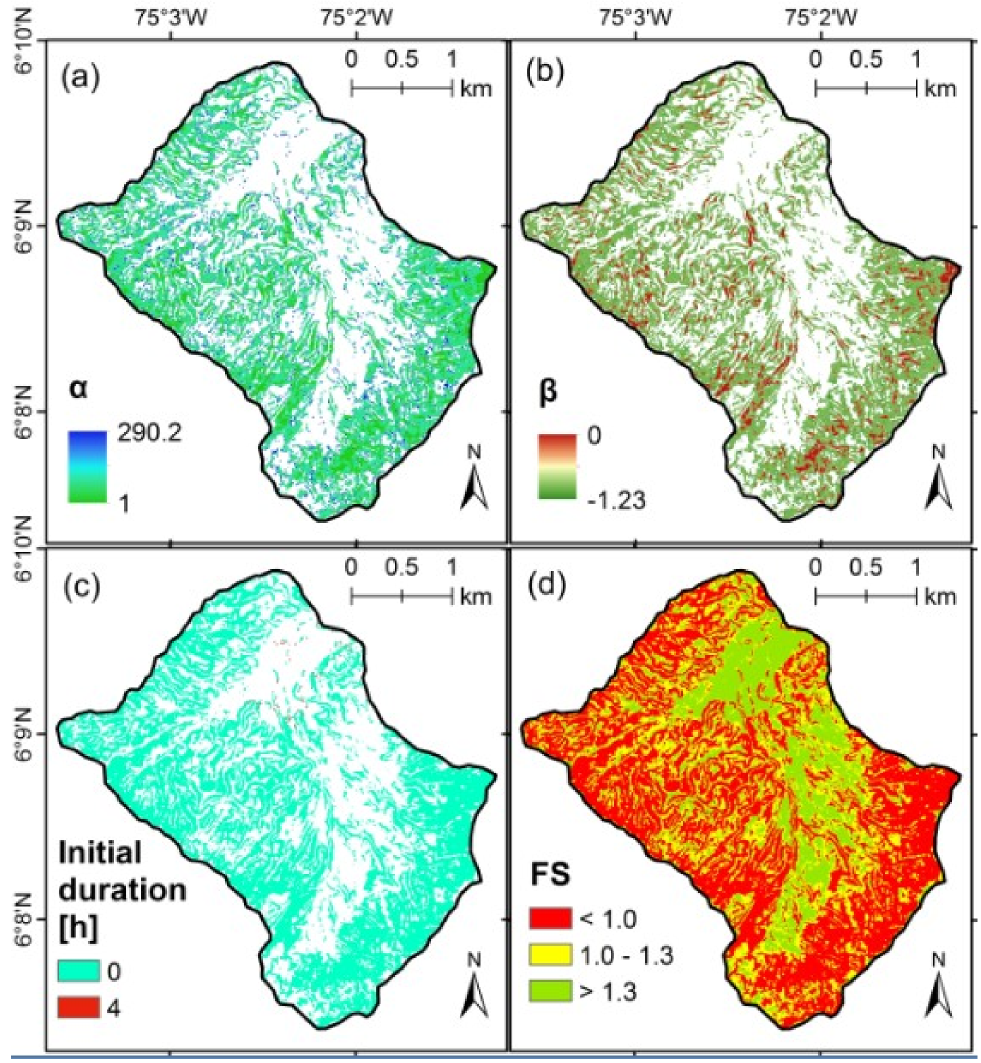

Fig. 8. Rainfall *I-D* thresholds (represented in maps) for grid cells of the La Arenosa basin, using M2: (a) scale parameter α, intercept in Eq. (6), (b) shape parameter β, slope in Eq. (6), and (c) initial duration (threshold), and (d) factor of safety map for a complete soil saturated scenario.

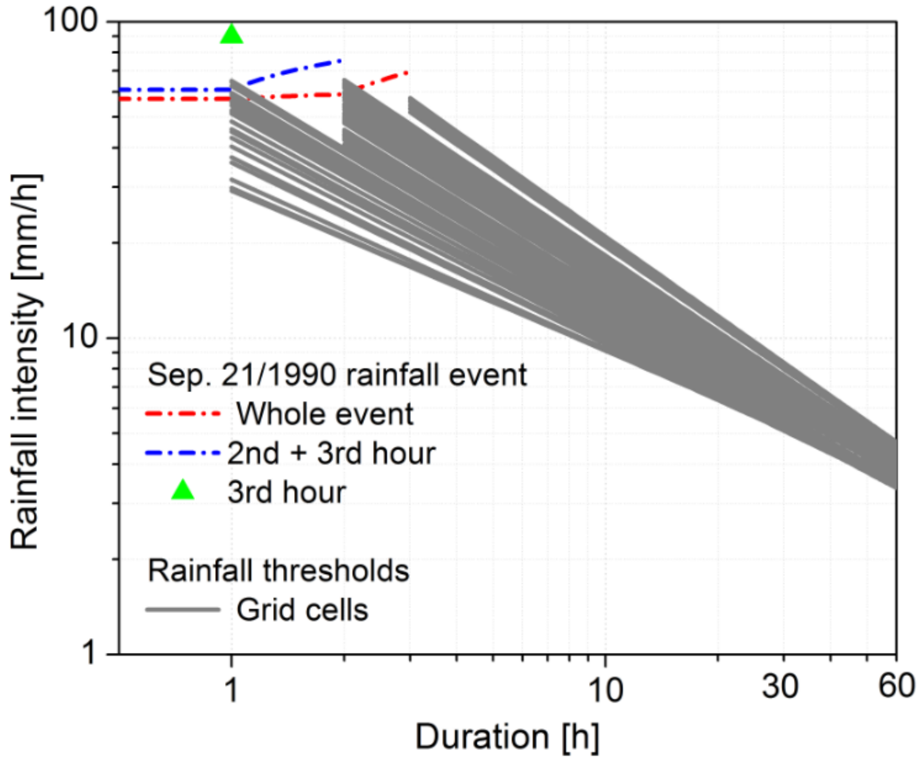

Fig. 9. Rainfall thresholds for 200 grid cells from the landslide scarp inventory of the La Arenosa 1990 event, using method M2.

941

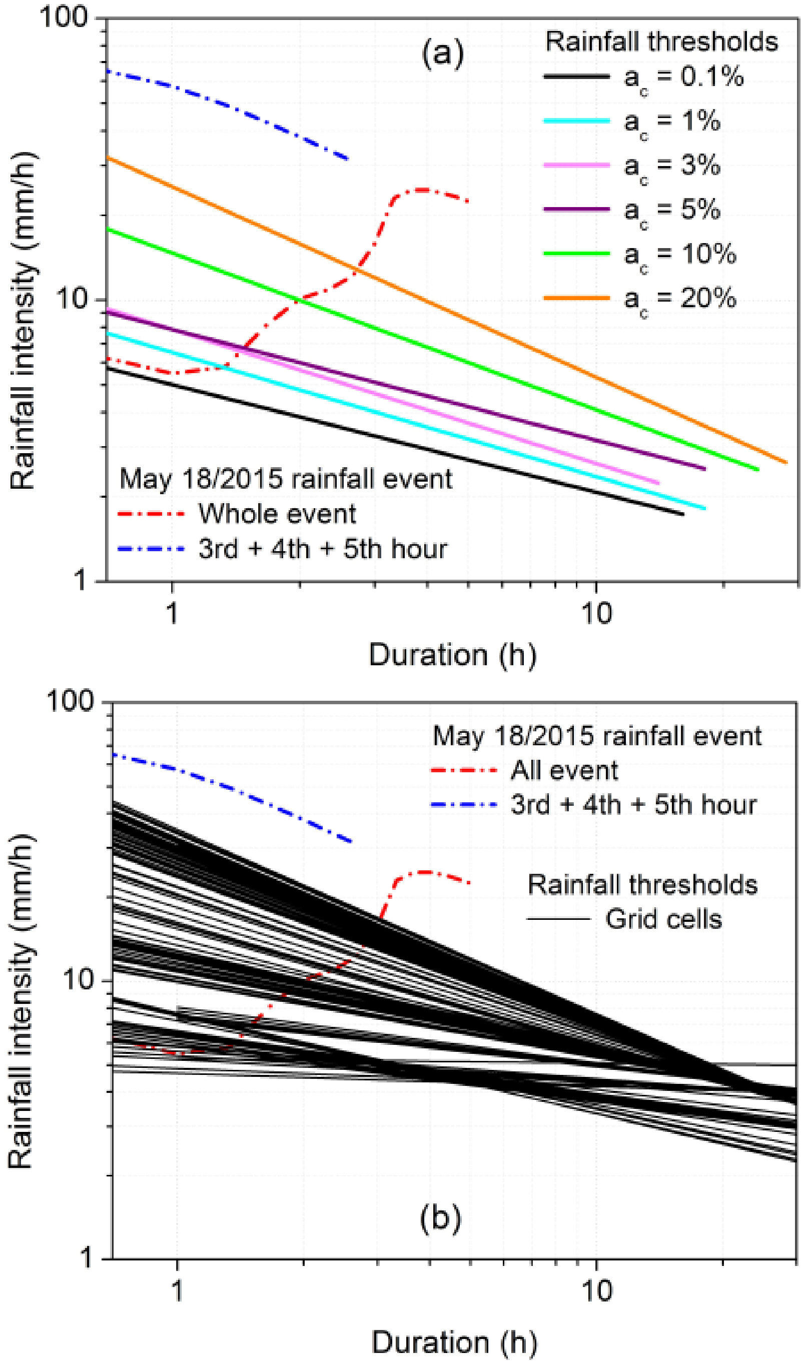

Fig. 10. Rainfall thresholds for the La Liboriana basin using: (a) method M1 for different a_c values; (b) method M2, for 240 grid cells from the landslide scarp inventory of the La Liboriana 2015 event.

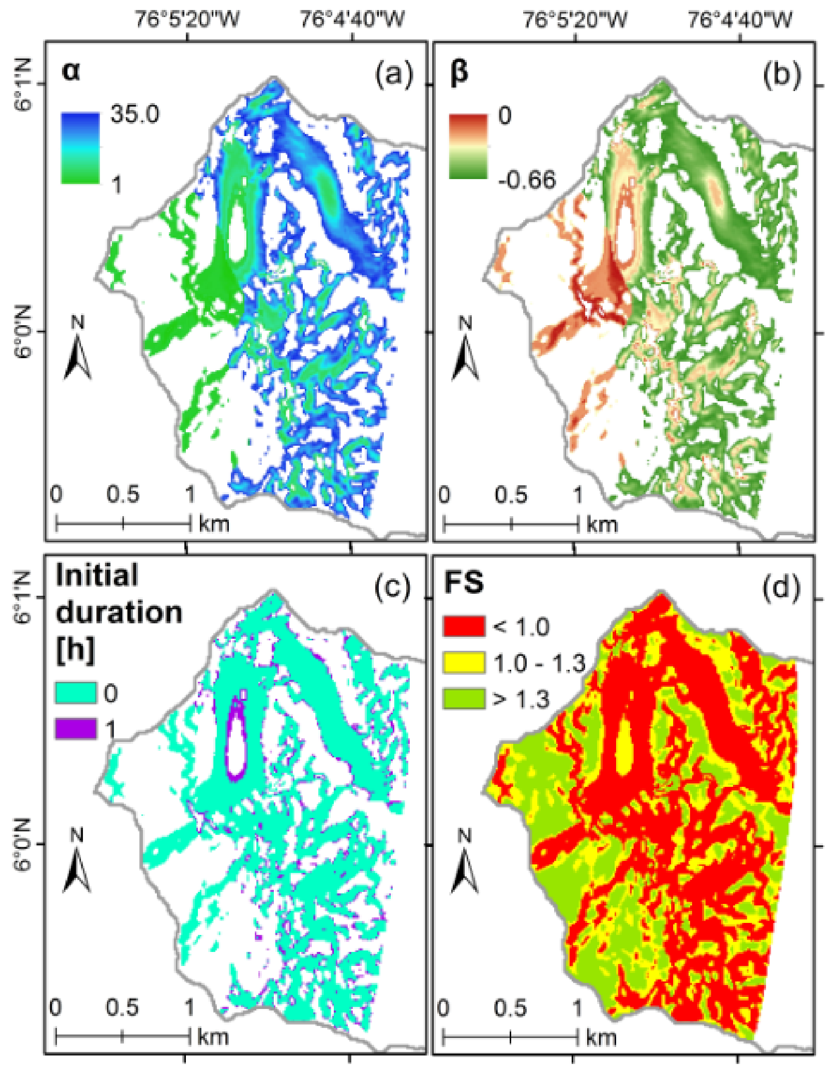

Fig. 11. Rainfall *I-D* thresholds (represented in maps) for grid cells of the La Liboriana basin, using M2: (a) scale parameter α, intercept in Eq. (6), (b) shape parameter β, slope in Eq. (6), and (c) initial duration (threshold), and (d) factor of safety map for a complete soil saturated scenario

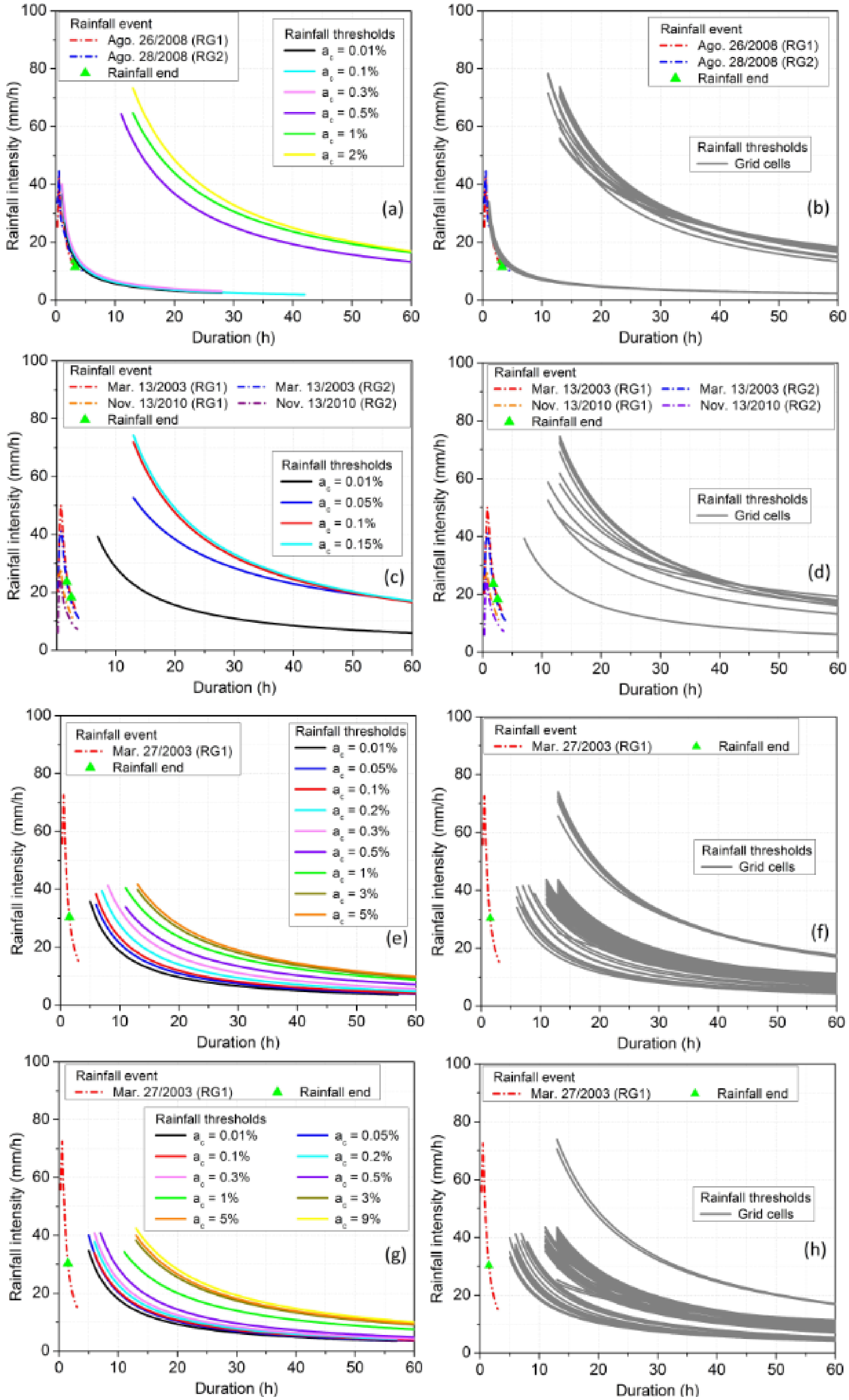
Rainfall event
Ago. 26/2008 (RG1)
Ago. 28/2008 (RG2)
Rainfall end
Rainfall thresholds
a_c = 0.01%
a_c = 0.1%
a_c = 0.3%
a_c = 0.5%
a_c = 1%
a_c = 2%
(a)
Grid cells
(b)
Mar. 13/2003 (RG1)
Mar. 13/2003 (RG2)
Nov. 13/2010 (RG1)
Nov. 13/2010 (RG2)
a_c = 0.05%
a_c = 0.15%
(c)
(d)
Mar. 27/2003 (RG1)
a_c = 0.2%
a_c = 3%
a_c = 5%
(e)
(f)
a_c = 9%
(g)
(h)
Rainfall intensity (mm/h)
Duration (h)

Fig. 12. Rainfall thresholds for the watersheds from Medellín using methods 1 and 2: watershed 1 (W1): (a) method M1 and (b) method M2; watershed 2 (W2): (c) M1 and (d) M2; watershed 3 (W3): (e) M1 and (f) M2; watershed 4 (W4): (g) M1 and (h) M2.

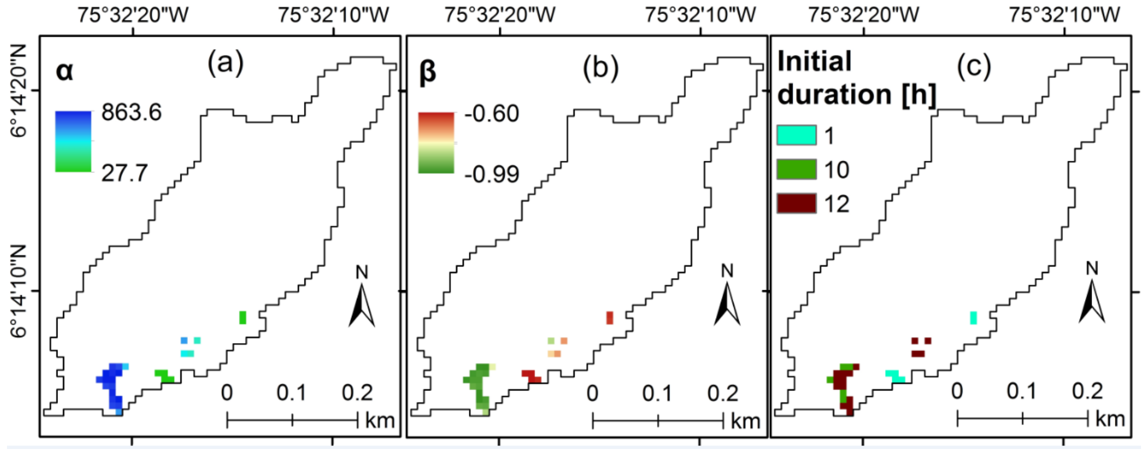

Fig. 13. Rainfall *I-D* thresholds (represented in maps) for grid cells of the watershed 1 (W1), using M2: (a) scale parameter α, intercept in Eq. (6), (b) shape parameter β, slope in Eq. (6), and (c) initial duration (threshold).

948

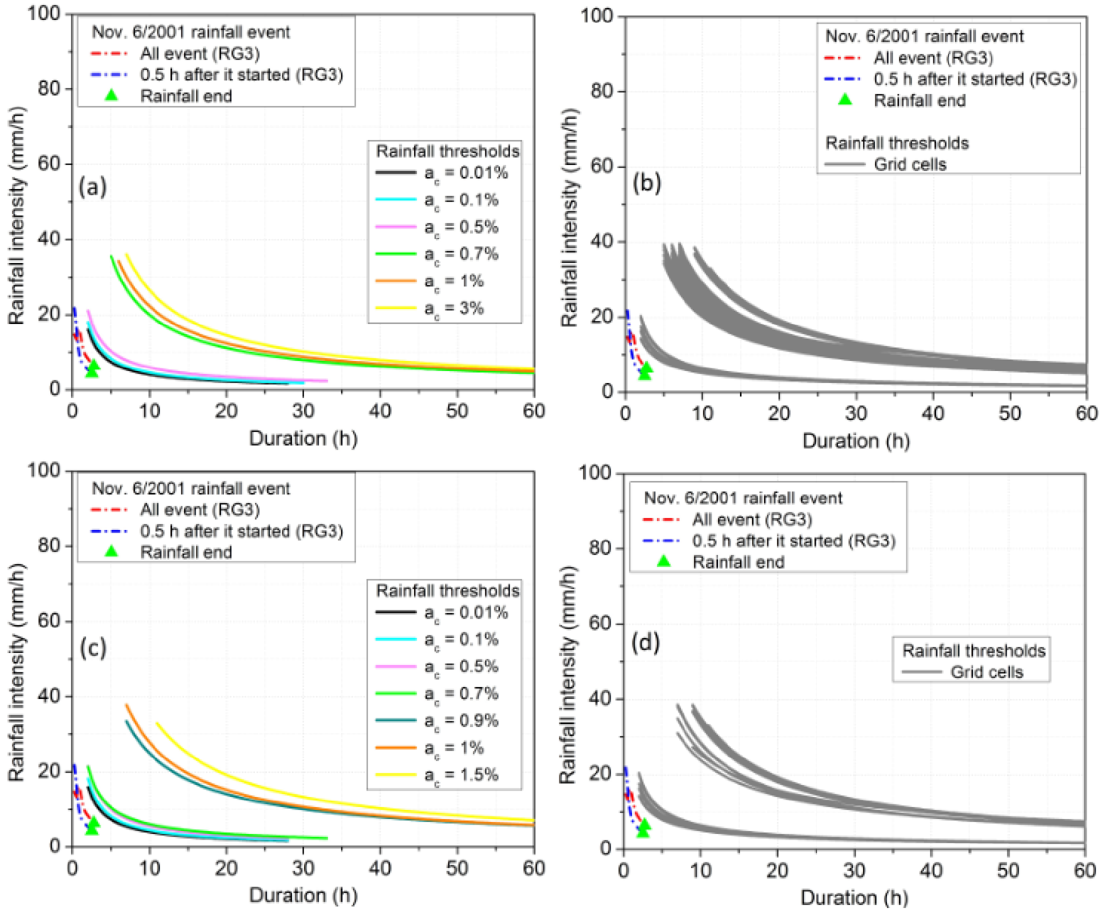

Fig. 14. Rainfall thresholds for the watersheds from San Antonio de Prado (Medellín) using methods M1 and M2: watershed 5 (W5): (a) M1 and (b) M2; watershed 6 (W6): (c) M1 and (d) M2.

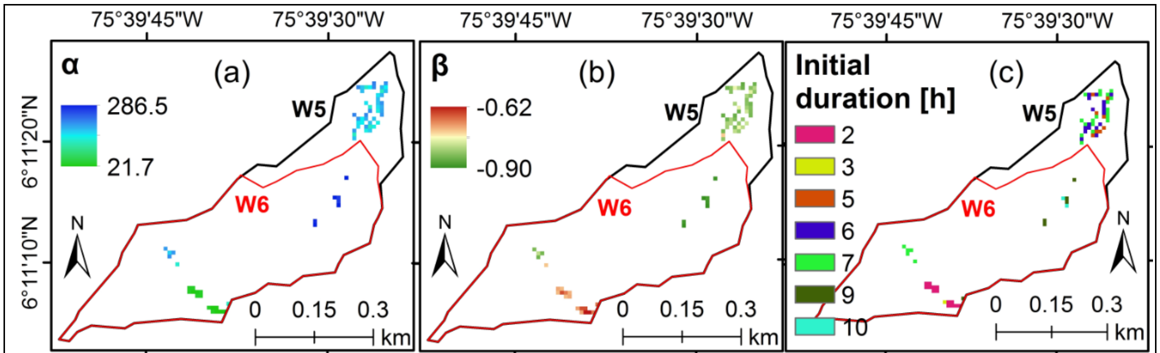

Fig. 15. Rainfall *I-D* thresholds (represented in maps) for grid cells of the watershed 5 (W5), using M2: (a) scale parameter α, intercept in Eq. (6), (b) shape parameter β, slope in Eq. (6), and (c) initial duration (threshold).